Research Paper

GEOSPHERE

GEOSPHERE

https://doi.org/10.1130/GES02900.1

13 figures; 2 tables

CORRESPONDENCE:
william.taylor@manchester.ac.uk

CITATION: Taylor, W.J., Hodgson, D.M., Peakall, J., Kane, I.A., Flint, S.S., Bouwmeester, M.J., Marsh, J.R., Soutter, E.L., Poyatos-Moré, M., McArthur, A.D., Keavney, E., Brunt, R.L., and Valdez-Buso, V., 2026, Spilling into confinement: Submarine canyon-confined overbank processes and architecture: Geosphere, https://doi.org/10.1130/GES02900.1.

Science Editor: David E. Fastovsky
Associate Editor: Lawrence Tanner

Received 9 June 2025
Revision received 14 October 2025
Accepted 28 November 2025

Published online 17 December 2025

Spilling into confinement: Submarine canyon-confined overbank processes and architecture

William J. Taylor[1,*], David M. Hodgson[1], Jeff Peakall[1], Ian A. Kane[2], Stephen S. Flint[2], Max J. Bouwmeester[2], Joshua R. Marsh[2], Euan L. Soutter[2], Miquel Poyatos-Moré[3], Adam D. McArthur[1], Ed Keavney[1], Rufus L. Brunt[2], and Victoria Valdez-Buso[4]

[1]School of Earth and Environment, University of Leeds, Leeds LS2 9JT, UK
[2]Department of Earth and Environmental Sciences, University of Manchester, Manchester M13 9PL, UK
[3]Departament de Geologia, Universitat Autònoma de Barcelona, 08193 Bellaterra (Cerdanyola del Vallès), Spain
[4]Departamento de Geologia, Universidade Federal do Paraná, 19001 Curitiba, Brazil
*Present address: Department of Earth and Environmental Sciences, University of Manchester, Manchester M13 9PL, UK

ABSTRACT

Submarine canyon-confined overbanks comprise substantial volumes of thin-bedded sediment gravity flow deposits that were either stripped or overspilled from adjacent channels and offer more complete records of canyon evolution than axial deposits. The Punta Baja Formation, Mexico, comprises a rare exhumed canyon fill with kilometer-scale dip and strike exposures that permit detailed documentation by high-resolution sedimentary logging and photogrammetric models. The lower overbank is characterized by laterally variable sandstone bed thicknesses and grain sizes, indicating that turbulent flows of varying magnitudes overspilled from channels. Thick sandstone beds contain paleocurrent indicator reversals and hummock-like bedforms, representing high-energy combined flows that deflected and reflected against the canyon margin. In the upper overbank, as the canyon fill aggraded and widened, fining- and thinning-upward packages developed, which decay in thickness and grain size away from the axis. Mud-rich packages contain mixed-grain-size bedforms, where abrupt lateral changes between different types of bedform support unusually rapid lateral flow transformations from turbulent to laminar over a distance of ~200 m. Beds with rhythmic bundles of silt-rich, mud-draped bedforms support reworking by internal tides. This study demonstrates that bed-scale analysis of confined overbanks can provide vital, yet commonly overlooked, records of submarine canyon evolution. We show that canyon-confined overbank successions are more diverse than their basinward counterparts because erosional confinement and dynamic internal topography promote a wider range of flow types and magnitudes. These findings suggest the existing twofold interpretation of internal levee or terrace deposits may be oversimplified in proximal overbank settings, where such deposits are unlikely to develop as discrete subenvironments.

William James Taylor https://orcid.org/0000-0002-1954-3924

INTRODUCTION

Submarine canyons are globally important as conduits for sediment and pollutant transfer from continents to deep-marine basins (Harris et al., 2014; Amaro et al., 2016; Mountjoy et al., 2018; Zhong and Peng, 2021; Chen et al., 2025; Keavney et al., 2025b). Particulates, including sediment, are primarily transported through canyons by sediment gravity flows, which can be powerful enough to sculpt the canyon floor by tens of meters in a single event (Heezen and Ewing, 1952; Conway et al., 2012; Mountjoy et al., 2018; Paull et al., 2018; Talling et al., 2023; Normandeau et al., 2025). Sediment can be further remobilized by internal tidal currents, which become focused and amplified within the steep walls of canyons (Petruncio et al., 1998; Hall et al., 2017; Li et al., 2019; Maier et al., 2019; van Haren et al., 2022). Canyon axes are channelized and commonly dominated by sediment bypass and erosion (Kneller, 2003; Stevenson et al., 2015; Bouwmeester et al., 2025), while their adjacent overbank environments within the main canyon confinement surface are sites of deposition and receive sediment from overspill and flow stripping via bypassing flows (Piper and Normark, 1983; Mutti and Normark, 1987; von Rad and Tahir, 1997; Babonneau et al., 2004; Paull et al., 2013; Clift et al., 2014). Consequently, canyon-confined overbank settings can accumulate substantial volumes of thin-bedded sediment gravity flow deposits (Deptuck et al., 2007; Paull et al., 2013; Jobe et al., 2015; Maier et al., 2018) and preserve a more complete, yet underutilized, record of sedimentary processes and system evolution than axial deposits (e.g., Hubbard et al., 2014, 2020; Jobe et al., 2017, 2024).

While many authors have documented the sedimentology of ancient canyon fills (e.g., Lowe, 1972; Stanley, 1975; Clifton, 1984; Morris and Busby-Spera, 1988; Millington and Clark, 1995; Cronin and Kidd, 1998; Anderson et al., 2006; Ito et al., 2014; Bain and Hubbard, 2016; McArthur and McCaffrey, 2019; Janocko and Basilici, 2021), studies are commonly biased toward better-preserved coarse-grained canyon axes, and few have fully considered the utility of canyon-confined overbanks as records of canyon evolution (e.g., Satur et al., 2005; Di Celma et al., 2010; Mercier et al., 2026). At present, much of the understanding of sedimentary processes in these environments is based

on studies of channel-levee systems in mid- to lower-slope settings, which recognize internal levee and terrace deposits (e.g., Kane and Hodgson, 2011; Hansen et al., 2015). These channel-levee models may not be representative of canyon-confined overbank settings. This is because canyons are more deeply incised, record deposition from flows with a short transport distance (Wynn et al., 2007; Babonneau et al., 2010; Hansen et al., 2015), and are susceptible to sediment resuspension and transport by internal tides (Shepard and Marshall, 1969; Shepard, 1976; Gardner, 1989). Furthermore, most studies have only considered deposition from fully turbulent sediment gravity flows. Observations from modern canyon overbanks (commonly referred to as terrace surfaces) identify a wide range of erosional and depositional relief generated by scours (Paull et al., 2013; Symons et al., 2016; Covault et al., 2017; Li et al., 2020) and mass-transport deposits (Tek et al., 2021; Pope et al., 2022; Talling et al., 2022; Ruffell et al., 2024). Therefore, sediment gravity flows, which are sensitive to variations in topography of different scales and orientations (e.g., Baas et al., 2011; Patacci et al., 2015; Soutter et al., 2021; Taylor et al., 2024), may interact with seabed relief and undergo rapid transformations in rheology and velocity, potentially adding substantial complexity to their deposits.

This study aims to document a rare example of an exhumed canyon-confined overbank from the Upper Cretaceous strata of the Peninsular Ranges forearc basin complex, Baja California, Mexico. The Punta Baja Formation represents a well-exposed canyon fill with good dip-oriented and strike-oriented exposures, which faced the Pacific Ocean in the Cretaceous (Boehlke and Abbott, 1986; Kane et al., 2022; Bouwmeester et al., 2025). The objectives of this study are to: (1) identify, describe, and interpret the canyon-confined overbank deposits; (2) detail their stratigraphic and spatial distribution within the overbank succession; and (3) evaluate the influence of canyon confinement and complex seabed topography on depositional environments and the spatio-temporal evolution of the canyon fill. Based on the results, we propose a new sedimentological model for canyon-confined overbanks, providing an effective tool to aid in reconstructions of deep-water processes and environments in modern and preserved sedimentary systems and thereby unlocking the deposits of canyon-confined overbanks as important records of canyon evolution.

GEOLOGICAL SETTING

The Peninsular Ranges Forearc Basin Complex

The Punta Baja Formation constitutes part of the Mesozoic Peninsular Ranges forearc basin complex (Fig. 1), which crops out along the Pacific coastal margin of northwestern Baja California, México, and southwestern California, USA (Gastil et al., 1975; Busby et al., 1998). The stratigraphy of the Peninsular Ranges forearc records the evolution of a long-lived convergent plate boundary from an extensional intraoceanic arc system in the Late Triassic, through a fringing island arc stage during the Early to mid-Cretaceous, to a highly compressional continental arc in the Late Cretaceous (Engebretson et al., 1985; Glazner, 1991; Busby et al., 1998).

The transition to a compressional stress regime was characterized by reverse faulting and uplift, followed by batholith emplacement and subsequent unroofing (Busby et al., 1998; Busby, 2004). Erosion of the arc basement rocks led to an influx of coarse sediment across a relatively narrow shelf into several ocean-facing forearc basins (Busby et al., 1998; Kimbrough et al., 2001). The orientation and spacing of submarine feeder canyons and slope channel-levee systems were dictated by right-lateral strike-slip deformation from oblique plate convergence (Busby et al., 1998; Kimbrough et al., 2001).

The Peninsular Ranges forearc stratigraphy (Fig. 1B) comprises: (1) pre-batholithic volcanic and carbonate rocks of the Alisitos Group (Busby, 2004); (2) post-batholithic fluvial channel fills, related deposits, and paleosols of the La Bocana Roja Formation (Kilmer, 1963); (3) deep-marine canyon-fill deposits of the Punta Baja Formation (Kilmer, 1963; McGee, 1965; Boehlke and Abbott, 1986); (4) shallow-marine and fluvial deposits of the El Gallo Formation (Kilmer, 1963; Renne et al., 1991); and (5) shallow shelf to deep-marine canyon and slope channel-levee complexes of the Rosario Formation (Morris and Busby-Spera, 1988, 1990; Kane et al., 2009; Hansen et al., 2017; Kneller et al., 2020). The stratigraphic alternation of nonmarine and deep-marine strata and their unconformable contacts point to alternating periods of uplift, basinward tilting, erosion, and subsidence, termed "porpoising" by Busby (2004). By the Paleocene, contraction of the forearc generated a broad syncline across the axis of the basin complex. This "pinned" the slope at relatively shallow marine depths and led to the deposition of conglomerates and lesser volcanic rocks of the Sepultura Formation (Busby, 2004).

The Punta Baja Formation

The Punta Baja Formation is interpreted as a submarine canyon fill (Kilmer, 1963; McGee, 1965; Boehlke and Abbott, 1986; Morris and Busby, 1996; Kane et al., 2022; Bouwmeester et al., 2025), which crops out around the village of Punta Baja, 17 km southwest of El Rosario (Figs. 1 and 2). The canyon system likely exploited structural lineaments in the underlying bedrock of the La Bocana Roja Formation, which underwent both syn- and postdepositional extensional and contractional deformation during the Cenomanian–Turonian, associated with the releasing and restraining bends of a dextral strike-slip fault zone (Kane et al., 2022; Bouwmeester et al., 2025). The oblique dextral strike-slip movement likely ceased by the time of sediment delivery to the canyon (earliest Santonian), given that the canyon fill was largely unaffected by syndepositional transpression (Kane et al., 2022).

The preserved canyon fill is up to ~120 m thick and 1.2 km wide, with downdip (5 km) and across-strike (2 km) constraints, and has a relatively wide grain-size range that comprises coarse- and fine-grained domains that represent the canyon axis and overbank environments, respectively (Fig. 3). The coarse domain comprises conglomeratic and sand-rich channel elements (e.g., Di Celma et al., 2011; McHargue et al., 2011) that record phases of westward lateral migration, characterized by numerous erosion surfaces, before a subsequent

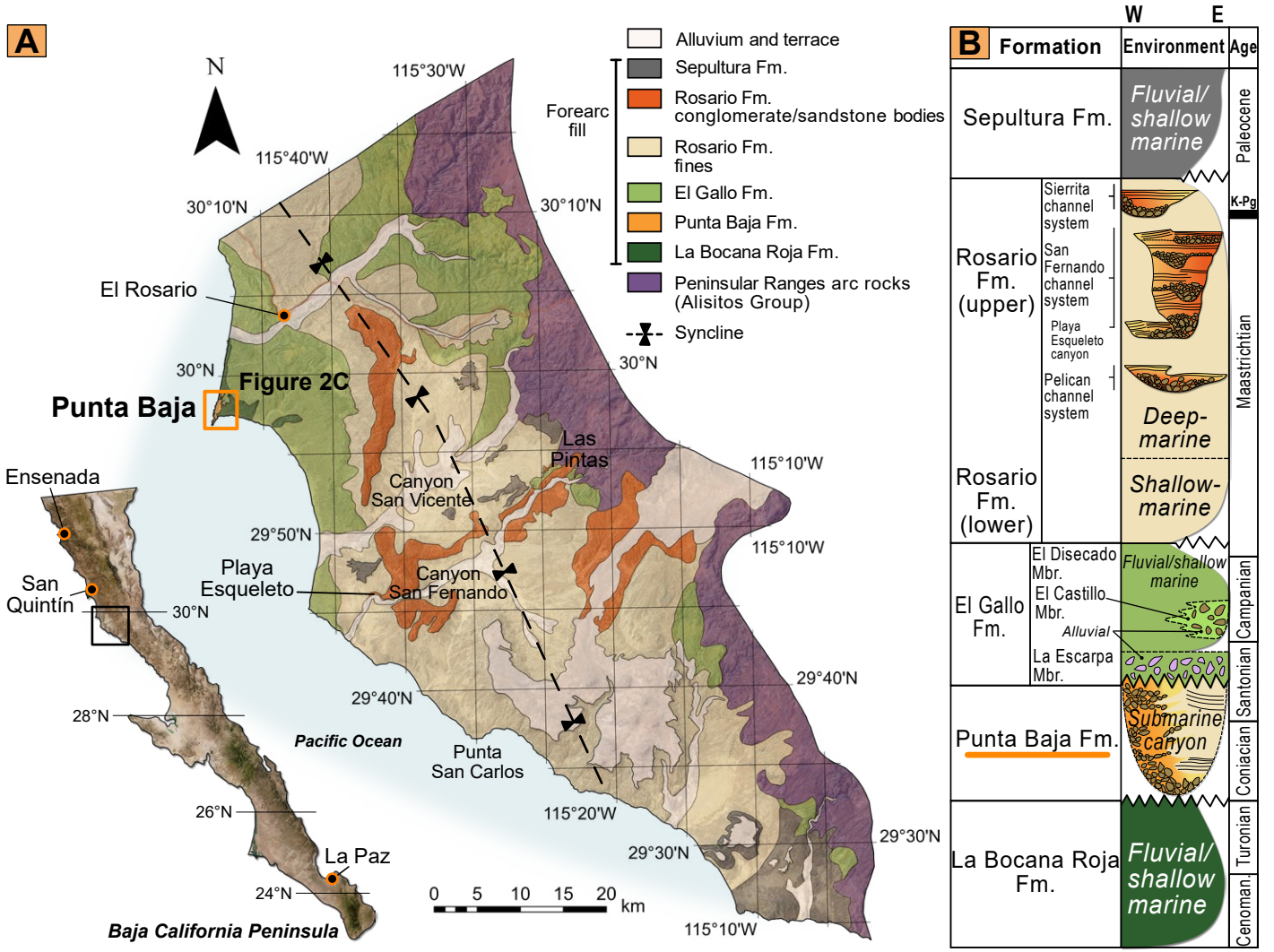

Figure 1. (A) Geological map of Rosario Embayment of Baja California, Mexico, showing main units of Peninsular Ranges forearc basin complex with study area highlighted in orange. Modified from Morris and Busby-Spera (1990) and Kneller et al. (2020). (B) Stratigraphic column of Rosario Embayment, summarizing main formations and depositional settings of Peninsular Ranges forearc basin complex. Drawings under "Environment" show the broad shape and architecture of each of the channel and canyon systems in the Rosario and Punta Baja formations and the distribution of their constituent coarser- and finer-grained lithologies. Modified from Kneller et al. (2020). K-Pg—Cretaceous-Paleogene boundary; Cenoman.—Cenomanian.

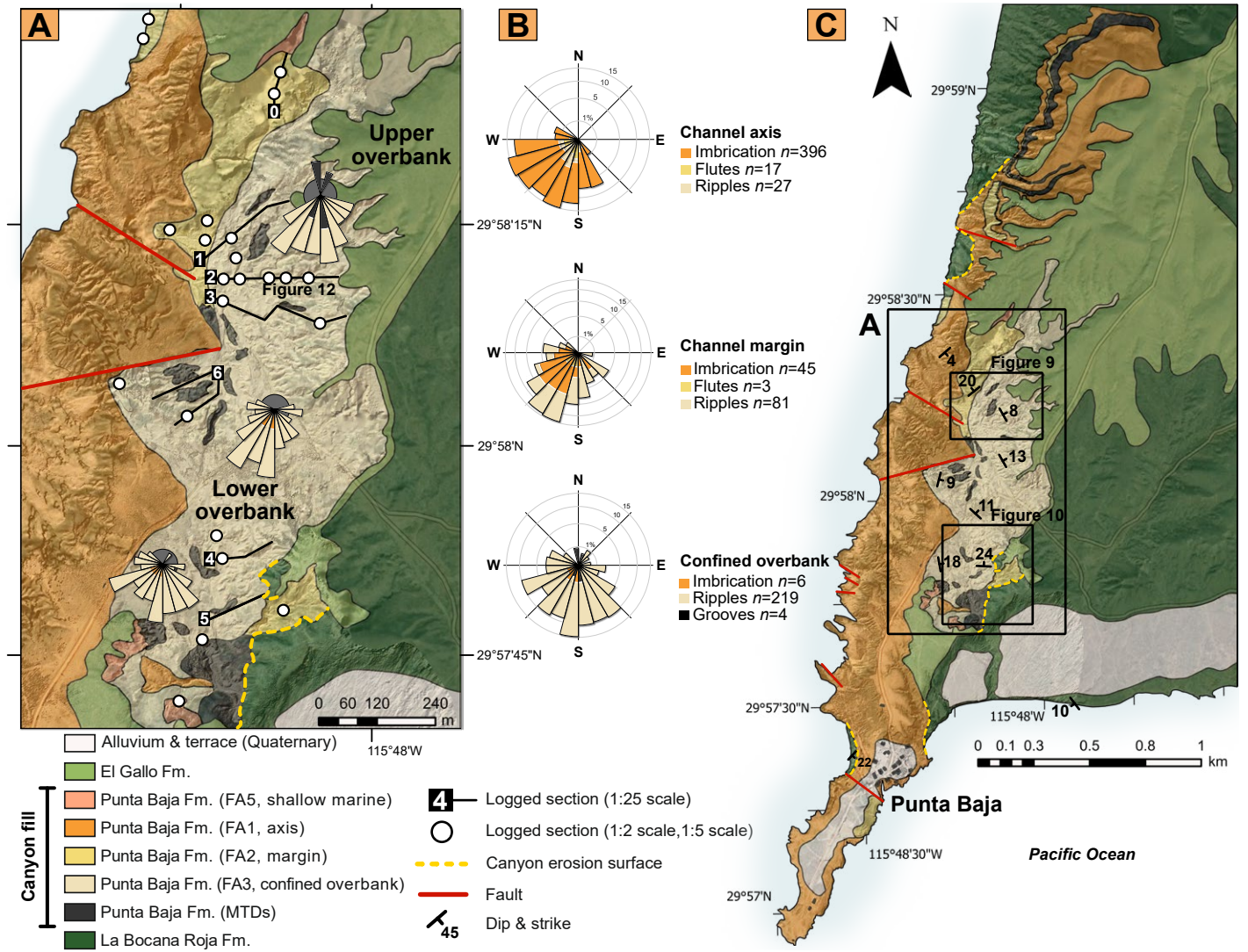

Figure 2. (A) Enlarged geological map of Punta Baja confined overbank (location shown in C). (B) Equal-area rose diagrams showing paleocurrent directions from conglomerate clast imbrication, flutes, grooves, and ripple foresets for each main facies association (FA). (C) Geological map of Punta Baja peninsula, with main formations and facies associations within Punta Baja Formation overlain onto a drone-captured digital elevation model. Map location is shown in Figure 1. MTDs—mass-transport deposits.

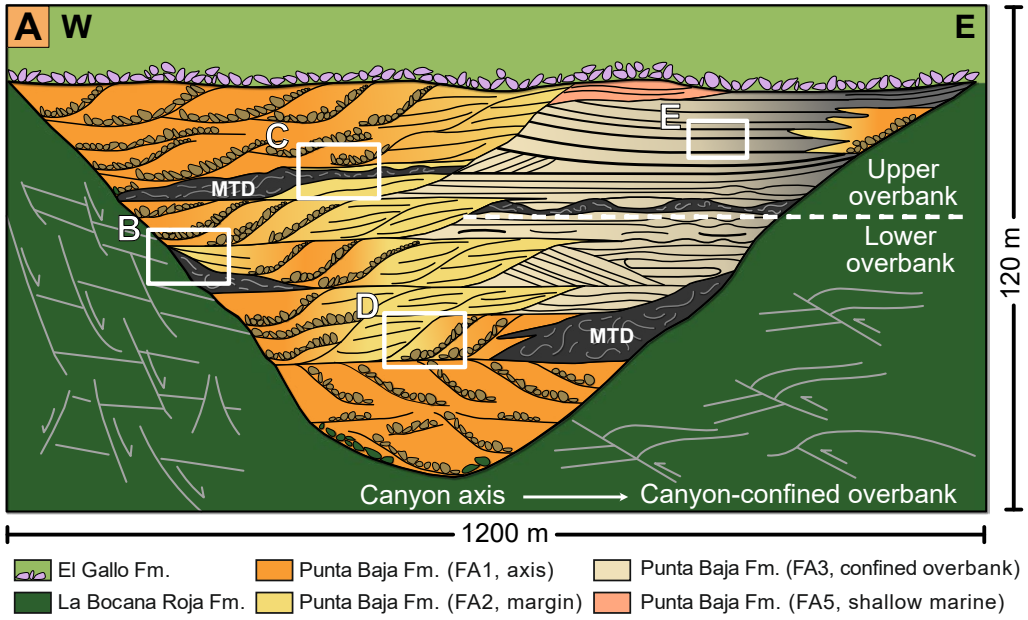

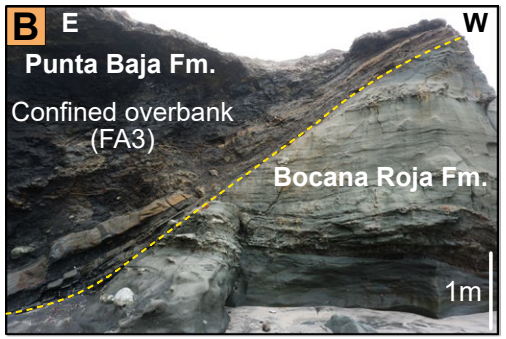

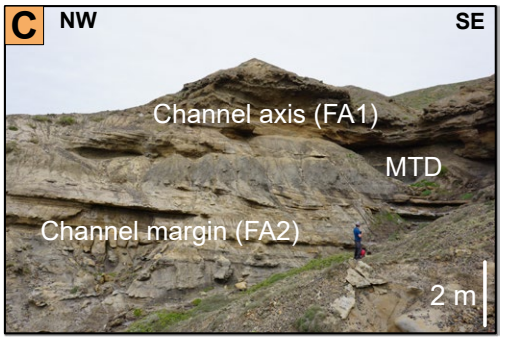

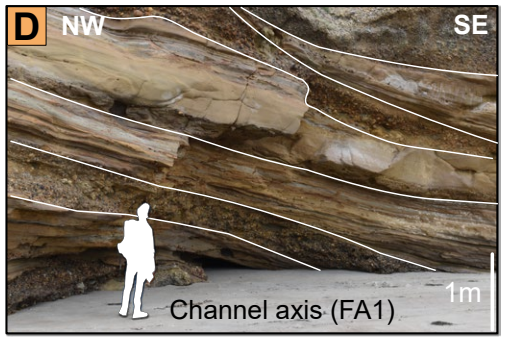

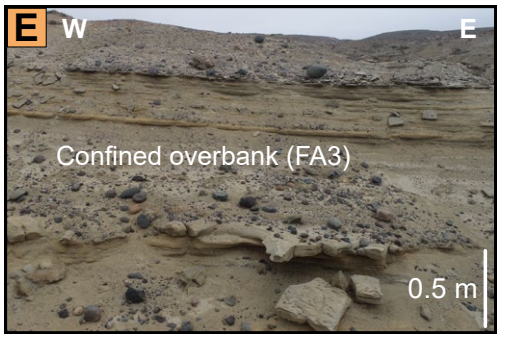

Figure 3. (A) Schematic cross section of Punta Baja canyon fill. (B–E) Photographs highlighting main facies associations (FA). (B) Confined overbank packages onlapping onto Bocana Roja Formation at western canyon margin. (C) Channel axis packages overlying mass transport deposits (MTDs) and channel margin packages. (D) Channel margin sandstone packages interbedded with axial conglomerates. (E) Confined overbank packages within upper overbank.

aggradational phase, represented by vertically stacked channel elements that onlap onto the western margin of the canyon (Fig. 3A; Boehlke and Abbott, 1986; Bouwmeester et al., 2025). Toward the east, the channel elements transition laterally into the fine-grained domain, which comprises a 30–70-m-thick succession of thin-bedded, heterolithic sandstones and mudstones, interpreted as the overbank, which onlaps onto the eastern canyon margin (Boehlke and Abbott, 1986). Regional paleoflow was to the southwest, with sediment gravity flows fed by material eroded from uplifted plutonic rocks of the Alisitos Group (Kane et al., 2022). The overlying El Gallo Formation sits unconformably on top of the Punta Baja Formation, characterized by an angular discordance marked by an extensive transgressive cobble lag deposit that represents a ravinement surface (Boehlke and Abbott, 1986; Kane et al., 2022; Bouwmeester et al., 2025).

METHODOLOGY

Dataset

This study focuses on the fine-grained domain of the Punta Baja canyon fill. The dataset comprises 36 sedimentary logs (301.5 m cumulative thickness), collected across strike and downdip, which capture spatial changes in facies and architecture (Fig. 2A). Logs were collected at 1:25 scale and correlated by walking out marker beds. These correlations were aided by interpretations of photogrammetric models captured by uncrewed aerial vehicle (UAV), covering an area of 2.3 km^2.

Where the exposure allowed, higher-resolution logs (between 1:2 and 1:5 scale) captured measurements of more than 2000 beds. Emphasis was placed on bed-scale changes in thickness, lithology, grain size, stratal boundaries, and constituent bedform types and their dimensions (including bedform amplitude and wavelength). Paleocurrent measurements (n = 798) were collected from clast imbrication, bedform foresets and planforms, ripple cross-lamination, and sole structures (flutes and grooves) from different parts of the canyon fill (Figs. 2A and 2B). Grain size was estimated in the field using a hand lens and a grain-size comparator card. Because clay- and silt-sized grains are difficult to measure accurately in the field, *mud* and *mudstone* are employed as general terms to describe argillaceous laminae and bands (Winterwerp and van Kesteren, 2004). The color of the deposit also gave a useful indication of grain size, given that darker-colored rock typically indicates elevated mud content.

Terminology

Hierarchy-based classification schemes help to characterize submarine canyon and channel fills (e.g., Mutti and Normark, 1987; Sprague et al., 2002, 2005; Di Celma et al., 2011; McHargue et al., 2011). At the largest scale, *canyon fill* describes the deposits contained within the main canyon erosion surface. These can be subdivided into two components: the *canyon axis* and the *canyon-confined overbank*. The Punta Baja canyon axis comprises a channel belt (Bouwmeester et al., 2025) that consists of stacked and partially preserved *channel elements*, each defined by a channel-form erosion surface and its infilling sediment (e.g., McHargue et al., 2011). Channel elements are further organized into *channel axis* and *channel margin* facies associations (e.g., Mutti and Normark, 1987; Sprague et al., 2005; McHargue et al., 2011; Bouwmeester et al., 2025). The canyon-confined overbank described herein comprises flows deposited outside of channel elements but within the main canyon erosion surface. Bed types are identified, which are interpreted to represent deposition from a single sediment gravity flow. Internal divisions are identified using sedimentary structures that rely on descriptive characteristics defined by Bouma (1962) and Lowe (1982). Canyon-confined overbanks are referred to geomorphologically as terraces or benches in modern systems, which are terms used to describe a relatively flat surface elevated above the canyon thalweg within the main canyon erosion surface (e.g., Babonneau et al., 2010; Maier et al., 2012). In ancient systems, canyon-confined overbanks are comparable to internal levee or terrace deposits (e.g., Kane and Hodgson, 2011; Hansen et al., 2015, 2017). We return to the nature of canyon-confined overbanks and how their stratigraphic relationships relate to modern geomorphic features in the Discussion section, utilizing the dataset presented herein.

SEDIMENTARY FACIES ASSOCIATIONS AND BED TYPES

The Punta Baja canyon-fill deposits were subdivided into four facies associations (Table 1; Fig. 3): FA1 (channel axis), FA2 (channel margin), FA3 (confined overbank), and FA4 (shallow marine). This study focuses on FA3, which constitutes the canyon-confined overbank setting. Nine bed types were identified in FA3, including high-density turbidity current deposits (HDTCDs 1 and 2), low-density turbidity current deposits (LDTCDs 1 and 2), transitional flow deposits (TFDs 1–3), internal tide-reworked deposits (ITDs), and mass-transport deposits (MTDs). These bed types have variable occurrence and distribution across the overbank, and individual beds can vary spatially in their character (Fig. 3). The bed types and their interpreted flow processes are described in the following subsections, with sketch logs and photographs shown in Figure 4. Facies associations for the axial parts of the canyon fill (FA1 and FA2) from Bouwmeester et al. (2025) provide further depositional context (Table 1).

High-Density Turbidity Current Deposits (HDTCDs 1 and 2)

Description

In the overbank, high-density turbidity current deposits (HDTCDs) are 15–50 cm thick (Fig. 4) and medium to coarse grained, with crude normal grading and erosional lower boundaries (2–10 cm relief) with rare groove marks on bed bases. Locally, they may contain subangular mudstone clast intervals or pebble lags in the lower 5–10 cm of beds. HDTCD 1 beds are tabular and comprise a

TABLE 1. FACIES ASSOCIATIONS (FA1–FA4), DESCRIPTIONS, AND ENVIRONMENT INTERPRETATIONS

Code	Facies association	Description	Interpretation	Photo
FA1	Thick-bedded conglomerate and sandstone packages	Highly amalgamated conglomerates (0.5–3.5 m thick) and sandstones (0.5–2.0 m thick). Conglomerates have strongly imbricated fabrics and are either clast supported and well sorted, or matrix supported and poorly sorted. They also have steep, erosional basal contacts. Beds are normally graded with rare inverse grading. They are sometimes cross-stratified (dune scale) and contain outsized clasts of the underlying La Bocana Roja Formation. Sandstones (very coarse to medium grained) are structureless, poorly sorted, and normally graded, with mud clasts at the bases of beds. Beds are tabular with erosive basal contacts and sharp top surfaces that can contain sporadic pebble cross-stratification. Packages are preferentially stacked towards the western canyon margin.	Channel axis and/or submarine braid plain (Hein and Walker, 1982; Klaucke and Hesse, 1996; Hesse et al., 2001; Bouwmeester et al., 2025), characterized by bedload deposits indicating scour, bypass, and fill from noncohesive debris flows. Interbedded sandstones and organized conglomerates indicate further deposition and prolonged reworking beneath turbulent high-density sediment gravity flows (Lowe, 1982). Amalgamation suggests multiple stages of scour, bypass, and fill as the system migrated laterally and aggraded. Preferential stacking of channel elements towards the western canyon margin may be in response to dominant extensional faulting and bedrock subsidence on that side and away from contractional features to the east (Kane et al., 2022).	Figs. 3C 3D, and 4A
FA2	Medium- to thick-bedded sandstone and thin-bedded mudstone packages	Weakly amalgamated sandstone beds (0.5–1.5 m thick), commonly interbedded with silt-rich mudstones (0.1–0.3 m thick) and minor conglomerates (<1 m thick). Sandstones (very coarse to medium grained) are moderately to well sorted and normally graded. Beds contain mud clasts and flame structures at the base, and sand-rich climbing ripples and planar lamination toward bed tops. Packages are typically fine grained, thin and decrease in dip angle upward and laterally over short distances (<10 m), and onlap onto steep erosion surfaces that truncate other sandstone packages. In some areas, packages are deformed, typified by slumped and rotated bedding.	Channel margin (Kane and Hodgson, 2011; Morris et al., 2016), characterized by rapid suspension settling from fully turbulent, high-density sediment gravity flows with sustained bedload transport (Bouma, 1962; Allen, 1971; Lowe, 1982). Sandstone packages were deposited within the confines of a channel element that migrated laterally westwards (Morris et al., 2016). Flame structures at the bases of sandstone beds are representative of syn- or postdepositional dewatering (Stow and Johansson, 2000). Mudstone clast intervals are interpreted as lag deposits, suggesting prolonged erosion (Kneller, 1995). Deformation indicates slumping and remobilization of soft sediments on unstable channel margins.	Figs. 3C
FA3	Medium- to thin-bedded, sand- and mud-rich heterolithic packages	Interbedded sandstone beds (0.01–0.9 m thick) and faintly laminated mudstone beds (0.01–0.7 m thick). Sandstones (very coarse to very fine grained) have variable bed characteristics and paleocurrent directions. Thin-bedded packages comprise normally graded, sharp-based sandstones that contain asymmetrical sand-rich current ripples, rounded biconvex ripples, and mixed-grain-size bedforms. Packages also contain rhythmic “bundles” of mud-draped wavy bedforms, starved laminae, and bidirectional flow indicators above sharp-topped turbidite beds. Thin-bedded packages are interrupted by outsized, erosive sandstone beds that contain structureless lower divisions (0.1–0.3 m thick) and planar laminated or hummock-like upper divisions (0.1–0.2 m thick). Locally, packages are disrupted by mass transport deposits (MTDs).	Confined overbank, characterized by turbidity currents (Bouma, 1962; Mutti, 1992), combined flows (Tinterri, 2011), turbulence-modulated transitional flows (Baas et al., 2009), and internal tides (Normandeau et al., 2024). High-density turbidity current deposits (HDTCDs) record channel-unconfined flows, and low-density turbidity current deposits (LDTCDs) record flows that were stripped or overspilled from channelized high- to low-magnitude turbidity currents, depositing hummock-like bedforms, which indicate flows that deflected off steep canyon walls (Tinterri et al., 2022). Transitional flow deposits (TFDs) are records of flow transformations from turbulent to laminar across the upper overbank, likely triggered by abrupt changes in flow confinement and/or entrainment of cohesive clay from mud-rich substrates (Baas et al., 2021a). See text for full interpretation.	Figs. 3B and 3E
FA4	Medium- to thick-bedded structured sandstones and sand-rich heterolithic packages	Thick-bedded sandstones (0.2–1.2 m thick) and thinly interbedded sandstones and mudstones. Sandstones (medium to very fine grained) are well sorted and normally graded. Beds contain abundant sand-rich bedforms that resemble hummocky cross-stratification (HCS). *Ophiomorpha* and *Thalassinoides* traces are common. Palynofacies consist of mixed opaques and amorphous organic matter with poor recovery and poor preservation, and deposits are rich in *Gonylacoid* cysts. Packages typically thicken upward before they are truncated by the overlying ravinement surface of the El Gallo Formation.	Shallow marine. Sand-rich HCS is typical of nearshore depositional environments (Harms, 1969). The upward-thickening trend might represent progradation of shoreface bars. Ichnofacies and palynofacies assemblages suggest a restricted shallow-marine environment. These packages are interpreted as transgressive deposits, preserved below the wave-ravinement surface of the El Gallo Formation, in the embayment that the Punta Baja canyon likely formed prior to deposition (Bouwmeester et al., 2025).	Bouwmeester et al. (2025, their figs. 5F, 5G, and 5I)

Note: Interpretations here form part of the study by Bouwmeester et al. (2025).

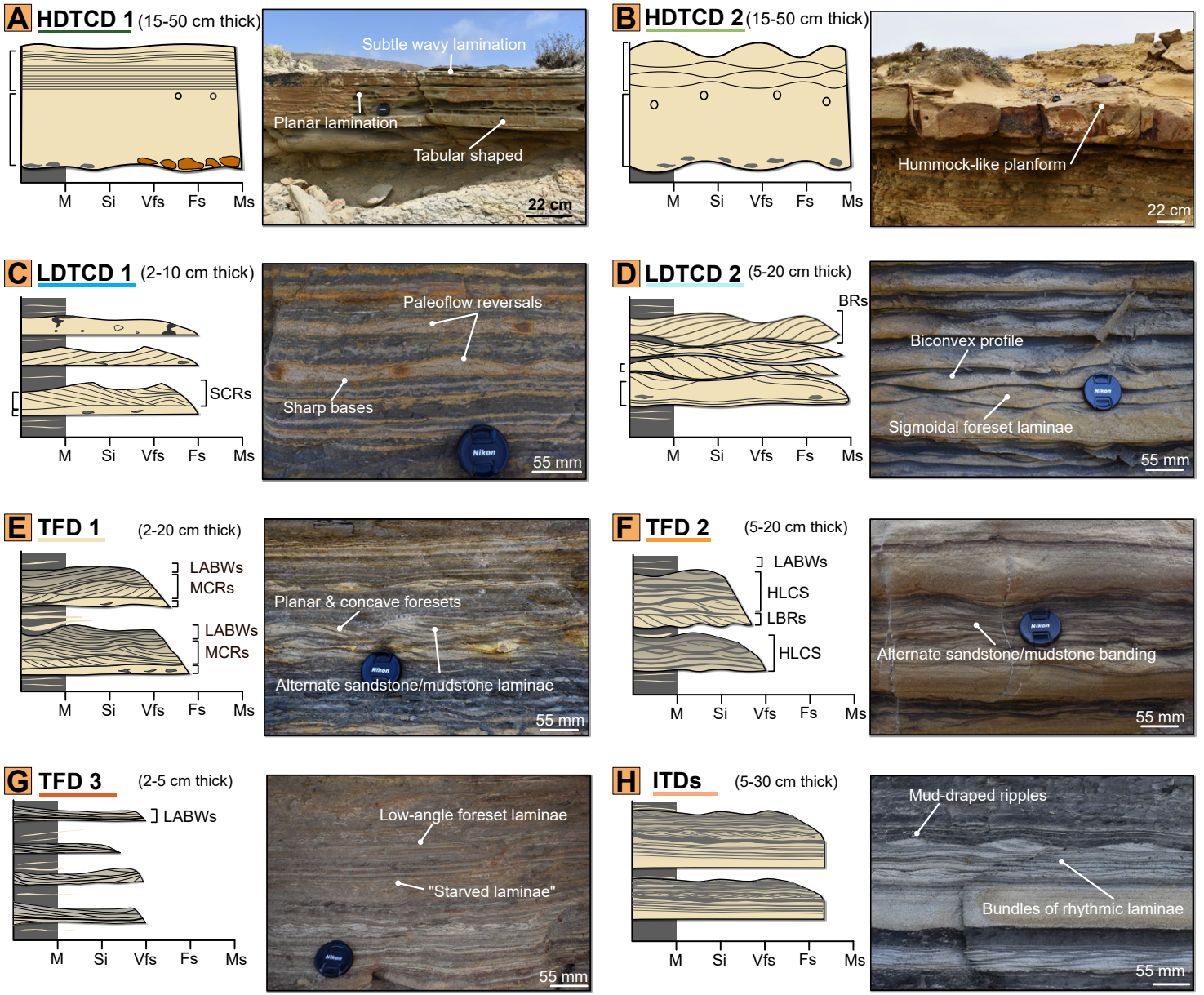

Figure 4. Sketch diagrams of beds and representative outcrop photographs that highlight internal divisions of: HDTCD 1 beds (A); HDTCD 2 beds (B); LDTCD 1 beds (C); LDTCD 2 beds (D); TFD 1 beds (E); TFD 2 beds (F); TFD 3 beds (G); ITDs (H). HDTCD—high-density turbidity current deposit; LDTCD—low-density turbidity current deposit; TFD—transitional flow deposit; ITD—internal tide-reworked deposit; SCRs—sand-rich current ripples; BRs—biconvex ripples; LABWs—low-amplitude bed waves; MCRs—mud-rich current ripples; HLCS—hummock-like cross-stratification; LBRs—large biconvex ripples; M—mud; Si—silt; Vfs—very-fine sand; Fs—fine sand; Ms—medium sand.

massive sand-rich division above the bed base (~20 cm thick) and pass upward into a thin sand-rich planar laminated upper division (<10 cm thick), with minor wavy and convoluted lamination at the top. HDTCD 2 beds are similarly characterized by a clean sand-rich lower division and erosional base but instead pass into an upper division of sand-rich, dune-scale swale- and hummock-like bedforms (Fig. 5; amplitude 10–24 cm, wavelength 56–80 cm). These form positive relief on bed tops, with mounded planform geometries (Fig. 4). Bioturbation is common in HDTCDs, with abundant *Ophiomorpha* and *Thalassinoides*.

Interpretation

HDTCD beds are interpreted as the deposits of high-density turbidity currents. The basal structureless divisions and crude normal grading within beds indicate rapid suspension fallout from a waning, high-density, fully turbulent flow (Kuenen, 1966; Lowe, 1982; Kneller and Branney, 1995; Sumner et al., 2008). The basal surfaces that truncate underlying strata, overlain by mud clast layers and pebble lags, indicate energetic flows that reworked, entrained, and bypassed substrate prior to deposition (Stevenson et al., 2015). The presence of grooves on bed bases represents bypassing of debritic heads or potentially previous debris flow events (Peakall et al., 2020; Baas et al., 2021b). The upper planar laminated division in HDTCD 1 beds likely indicate more dilute flow conditions via the migration of low-amplitude bedload sheets (Allen, 1984; Best and Bridge, 1992) or high-concentration conditions from the repeated formation and collapse of near-bed traction carpets (Kuenen, 1966; Sohn, 1997; Vrolijk and Southard, 1997; Sumner et al., 2008). Wavy and convolute lamination may indicate soft-sediment deformation of planar lamination shortly after deposition (Gladstone et al., 2018) or high rates of suspension settling over inactive bedforms forming "sinusoidal lamination" (Jopling and Walker, 1968; Ashley et al., 1982). HDTCD 2 beds similarly record deposition from high-density turbidity currents given their basal, sand-rich massive divisions but with an additional combined flow component, as reported by Keavney et al. (2025a). In submarine settings, beds with distinct hummock-like bedforms have been interpreted as combined flow deposits from reflection and deflection processes against basin-scale topography (Pickering and Hiscott, 1985; Tinterri, 2011; Bell et al., 2018; Hofstra et al., 2018; Tinterri et al., 2022; Keavney et al., 2025a).

Low-Density Turbidity Current Deposits (LDTCDs 1 and 2)

Description

Low-density turbidity current deposits (LDTCDs; 2–15 cm thick) comprise normally graded, fine- to very fine-grained sandstone. LDTCDs have a thin (2–5 cm thick), lower structureless sand-rich division with rare planar lamination and a sharp lower boundary, which passes upward into a division of

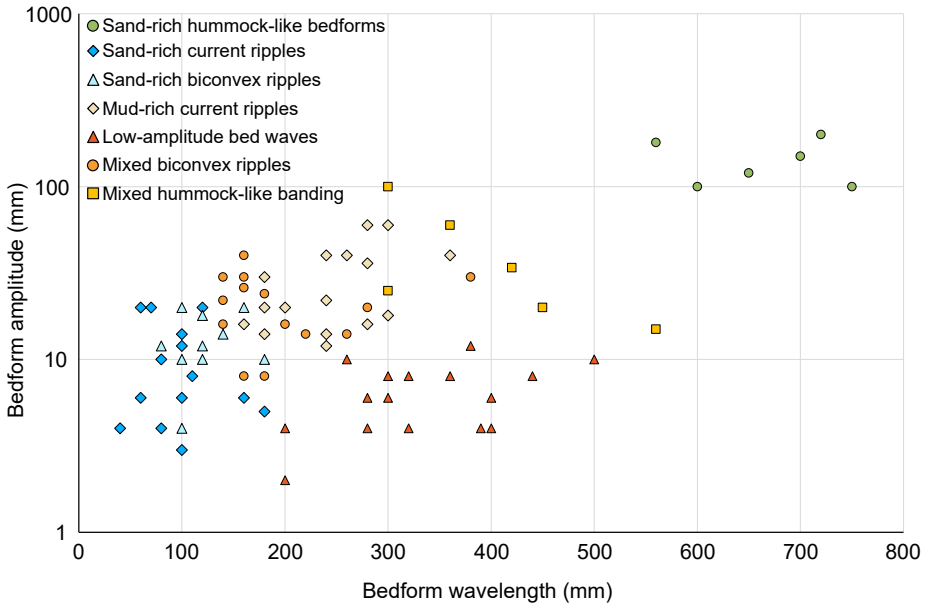

Figure 5. Graph showing average wavelengths and amplitudes of different bedform types observed within turbulent and transitional flow beds throughout Punta Baja confined overbank. Bedform amplitude is plotted with logarithmic scale.

sand-rich bedforms (Fig. 4). LDTCD 1 bedform divisions comprise low-angle climbing, asymmetric sand-rich current ripples (Fig. 5; amplitude 4–20 mm, wavelength 40–180 mm), with concave-up or planar foreset laminae with high termination angles (~40°) against the bases of laminasets. Conversely, LDTCD 2 bedform divisions are characterized by sand-rich biconvex ripples (Fig. 5; amplitude 4–30 mm, wavelength 80–180 mm), with symmetrical to slightly asymmetrical rounded profiles with a "pinch and swell" geometry. Biconvex ripples are either low- or high-angle climbing with stoss-side preservation. Internally, foreset laminae are sigmoidal shaped and drape slightly erosional lower bounding surfaces (1–2 cm deep). LDTCD 2 beds commonly exhibit a wide range of paleocurrent directions and reversals in their bedform divisions. Both LDTCD types have moderate to high bioturbation intensity, with abundant *Scolicia* and *Phycosiphon*. LDTCDs generally grade normally into an upper mudstone division, characterized by subtle siltstone lamination.

Interpretation

LDTCDs record deposition from low-density turbidity currents. The thin, structureless lower divisions and normal grading within beds indicate suspended-sediment fallout and layer-by-layer incremental deposition from a waning, dilute turbulent flow (Bouma, 1962; Mutti, 1992; Talling et al., 2012). The overlying sand-rich current ripples indicate deposition under sustained bedload transport (Allen, 1973) and lower rates of suspension settling than HDTCD beds (Jobe et al., 2012). They also resemble "sandy current ripples" of Baker and Baas (2020), further suggesting that they formed under fully turbulent conditions. LDTCD 2 beds likely record deposition under combined flows, consisting of oscillatory flows and a strong unidirectional flow component (up to 180° to the wave direction). These flows produce the sand-rich biconvex ripples and sigmoidal-shaped foresets through redistribution of sand by vortices on the lee side of the ripple related to the uneven forward and backward strokes of the oscillatory flow components. The top of the lee side of the ripple becomes preferentially "nourished" by sand and ultimately generates the rounded, biconvex profile. In submarine settings, these flow components have been attributed to flow interactions with subtle seabed topography (Tinterri, 2011, 2025), such as scours or bedform-scale relief (Ge et al., 2017; Hofstra et al., 2018). Upper mudstone divisions possibly indicate the distal expression of sediment gravity flow deposition, given the presence of subtle siltstone laminae (Boulesteix et al., 2019, 2022).

Transitional Flow Deposits (TFDs 1, 2, and 3)

Description

Transitional flow deposits (TFDs) are defined following Privat et al. (2024) as beds with transitional flow components but lacking debritic components associated with hybrid event beds. Here, TFDs (2–20 cm thick) are normally graded, fine- to very fine-grained sandstones and siltstones, with sharp to slightly erosional lower boundaries (Fig. 4). They are distinct in that they contain divisions of mixed-grain-size bedforms, which comprise alternations of sand-rich and poorly sorted mud-rich laminae and bands (Taylor et al., 2024).

TFD 1 beds typically have a lower structureless, sand-rich division (1–2 cm thick) with sporadic mud clasts and an upper division of large, asymmetrical mud-rich current ripples (Fig. 5; amplitude 10–60 mm, wavelength 160–360 mm). Their internal foreset laminae are thin (1–2 mm) and concave shaped and consist of alternating very fine-grained sandstone and mudstone. The climb angle of constituent laminae progressively increases upward, with concomitant bedform wavelength increase and bedform amplitude decrease, before passing into an upper mixed-grain-size bedform division of low-amplitude bed waves (LABWs; Baas et al., 2016; Fig. 5; amplitude 2–12 mm, wavelength 200–500 mm). These thin, asymmetrical bedforms contain gently dipping and alternating sandstone-mudstone foreset laminae.

TFD 2 beds (5–20 cm thick) have weakly erosional lower boundaries and comprise a structureless argillaceous lower division with mud clasts and an upper division of mixed-grain-size bedforms with markedly different geometries than those of TFD 1 beds. These divisions comprise larger mud-rich biconvex ripples (Fig. 5; amplitude 8–40 mm, wavelength 140–380 mm), with mixed sandstone-mudstone sigmoidal-shaped foreset laminae, and swale- and hummock-like cross-stratification (HLCS) banded sets (Taylor et al., 2024). HLCS banded sets comprise alternating sandstone-mudstone, concave-up and convex-up bands (>5 mm thick), which represent small-scale swale- and hummock-like features, respectively. Internally, bands either drape lower bounding surfaces tangentially at low angles (<10°) or are otherwise fully continuous throughout individual banded sets. Upward transitions between large biconvex ripples and HLCS banded sets are typically gradual and continuous, with only minor erosion observed between some laminae and banded sets. TFD 2 beds typically pass upward into thick, massive mudstone caps.

TFD 3 beds are between 2 cm and 5 cm thick and are observed isolated in thicker mudstone packages (Fig. 4). They are sharp based and comprise very thin, gently dipping sandstone-mudstone laminae (<2 mm thick). These features resemble LABWs like the upper divisions of TFD 1 beds but without lower mud-rich current ripple divisions. LABWs typically pass upward into very thin, laterally discontinuous sand-rich laminae that pinch out over 10 cm, forming a streaky texture above the bedform. Most TFD beds grade normally into a mudstone division, characterized by subtle siltstone laminae.

Interpretation

TFDs comprise mixed-grain-size bedforms with elevated proportions of mud in their laminae and banded sets. Currently, there are two process models that explain the origin of mixed-grain-size bedforms in sandstones: episodic near-bed turbulence damping (Lowe and Guy, 2000) and bedform development under mud-laden transitional flows (Baas et al., 2009, 2016; Stevenson

et al., 2020). Lowe and Guy (2000) proposed that mixed-grain-size bedforms develop at the bases of flows that vary between turbulent and laminar regimes through the cyclic development of near-bed cohesive plugs. These plugs were hypothesized to form through episodic damping of near-bed turbulence through electrical charge-induced bonding of clays following disaggregation of clay flocs (Lowe and Guy, 2000). Examples of bedforms formed under these conditions are reported from the Lower Cretaceous Britannia Formation (North Sea) and comprise banded divisions of clean sandstone and mudstone up to several meters thick containing abundant synsedimentary dewatering features such as sheared pipe and dish structures (Lowe and Guy, 2000).

While the mixed-grain-size bedforms documented in this study share some affinity with the banded divisions of Lowe and Guy (2000), they bear closer resemblance to the thin and sharp heterolithic laminae produced in the experiments of Baas et al. (2016), formed underneath transitional flows. Furthermore, the constituent grain sizes of laminae and bands observed here are more mixed (comprising "dirty" laminae and bands rather than clean sandstone) and lack prolific dewatering structures, which suggests that they were more likely the product of mud-rich transitional flows with sustained periods of traction (Baas et al., 2016).

Transitional flow behavior requires consideration of the balance between flow velocity–controlled turbulent forces and clay-derived cohesive forces (Baas et al., 2009; Sumner et al., 2009). On undergoing deceleration, cohesive clay particles in suspension form flocs and gels due to electrostatic forces between individual particles, which act to increase flow yield strength and viscosity and modulate flow turbulence (Wang and Plate, 1996; Baas and Best, 2002; Haughton et al., 2003; Talling et al., 2004). This initiates a transitional flow, characterized by a laminar plug-flow region with a lack of turbulence, which expands downward from an interval of low flow shear stress, as cohesive forces increase (sensu Baas et al., 2009).

TFD 1 beds are therefore interpreted to have formed under unidirectional transitional flows. The lower division of mud-rich current ripples resembles bedforms deposited under rapidly decelerated turbulence-enhanced transitional flow and lower transitional plug flow conditions (Baas et al., 2016; Baker and Baas, 2020). Here, a local turbulence enhancement from increased cohesive forces promoted larger bedforms (compared to sand-rich current ripples) before turbulence damping, which resulted in the gradual increase in bedform wavelength and reduction in bedform amplitude. The upper LABW division indicates deposition under rapidly decelerated upper transitional plug flow conditions (Baas et al., 2016; Baker and Baas, 2020), given that further increases in cohesion result in much longer, thinner bedforms (Stevenson et al., 2020). The gradual transition between mud-rich current ripples and LABWs in a single bed suggests progressive flow transformation from turbulent to laminar as the plug flow region expanded downward (Baas et al., 2021a; Taylor et al., 2024). TFD 1 beds are therefore interpreted to have formed at locations where turbulent flows were forced to decelerate and potentially where flows entrained cohesive mud.

TFD 2 beds record flow transformations under combined transitional flows. Here, flows underwent reflection, deflection, and ponding processes above subtle seabed topography, as with LDTCD 2 beds, but produced mixed-grain-size bedform sequences (Taylor et al., 2024). Upon interaction with topography, transitional flows take on the dynamics of a combined flow and deposit and rework sediment into large, mud-rich biconvex ripples (under turbulence-enhanced and lower transitional plug flow conditions) and HLCS banded sets (under upper transitional plug flow conditions). Mudstone caps further suggest deposition in topographic lows (Pickering and Hiscott, 1985; Haughton, 1994). Therefore, TFD 2 beds are indicators of flow transformation from interactions with topography while undergoing rapid deceleration over mud-rich substrates.

TFD 3 beds record rapidly decelerated upper transitional and quasi-laminar plug flow conditions. The presence of LABWs and their isolation in thick mud-rich packages supports an interpretation of higher mud content in the decelerating flow, suggesting higher flow viscosity and substantial sediment fallout from suspension while maintaining traction (Baker and Baas, 2020; Stevenson et al., 2020). The absence of the lower mud-rich current ripple divisions found in TFD 1 beds suggests that flows had decelerated and became too slow moving for lower transitional plug flow conditions or that flow transformation was too rapid to produce divisions of mud-rich current ripples.

Internal Tide-Reworked Deposits (ITDs)

Description

Internal tide-reworked deposits (ITDs; 5–30 cm thick) have sharp bases overlain by a lower sand-rich structureless division and an upper planar or wavy laminated and banded division (Fig. 6). The lower sand-rich division is typically sharp-topped, recording an abrupt change in grain size. Above this, the deposit is characterized by a division of wavy fine sandstone and siltstone laminae and bands that form distinct sand-mud "couplets" (Fig. 6C). These divisions differ from the banded divisions of TFD beds in that they form distinct bundles of thicker sandstone-mudstone bands (>5 mm) and thinner sandstone-mudstone laminae (1–2 mm). Mud-draped starved ripples that truncate laminae bundles are also observed. These bear resemblance to mud-rich current ripples in that they contain mixed sandstone-mudstone foreset laminae, but they are much smaller in size (amplitude 6–30 mm, wavelength 60–140 mm) and do not form high-angle climbing laminasets. The ripples are draped by mudstone and thin silt-rich laminae. Laterally discontinuous siltstone laminae that pinch out over 1–2 cm are observed near the top of the deposit before passing into ungraded mudstones (Fig. 6A).

Interpretation

ITDs resemble sediment gravity flow deposits that have been reworked by internal tides (May and Warme, 2000; He et al., 2011; Maier et al., 2019; Normandeau et al., 2024). The structureless divisions within ITD beds suggest

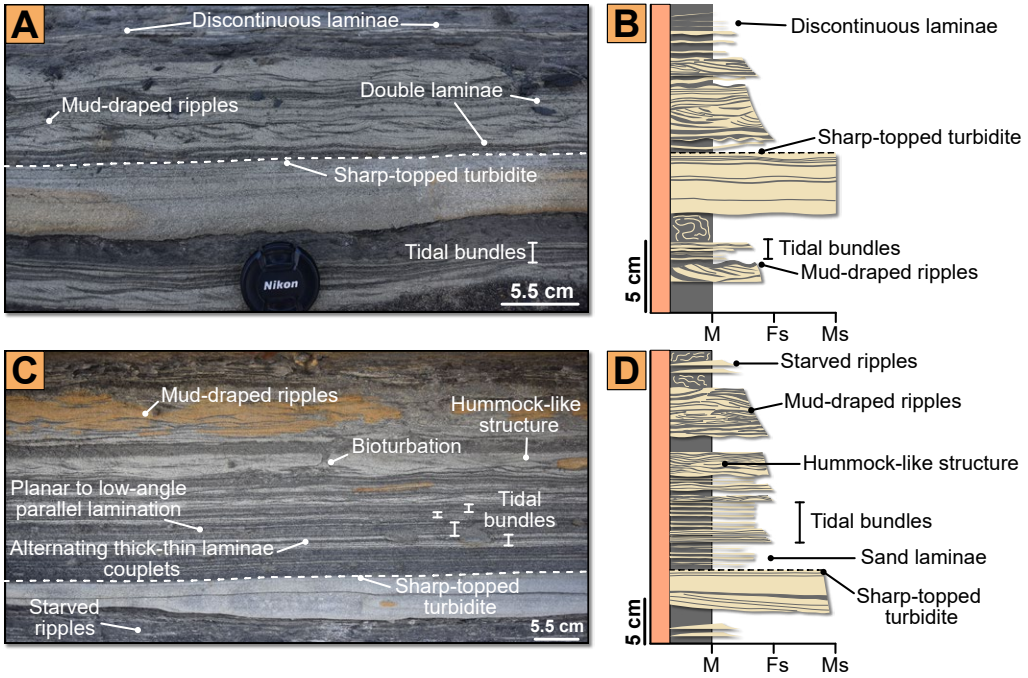

Figure 6. Annotated photographs (A, C) and sketch logs (B, D) of an outcrop section from upper confined overbank of Punta Baja Formation, highlighting characteristics of internal tide-reworked deposits similar to those of modern examples, including sharp-topped turbidites, mud-draped ripples, and bundles of thick-thin planar lamination. M—mud; Fs—fine sand; Ms—medium sand.

deposition from waning turbidity currents. However, their sharp tops, grain-size breaks, and upper divisions of cyclical laminated and banded bundles suggest reworking by internal tidal currents (Normandeau et al., 2024). The grain-size breaks at the top of sharp-topped beds might indicate bypass of the fine-grained fraction of a sediment gravity flow downslope (Stevenson et al., 2013) or internal tides either preventing the fine-grained tail of turbidity currents from settling or subsequently winnowing the turbidite after deposition. The alternation of sand- and mud-rich double laminae in the upper division is interpreted to record waxing and waning tidal cycles (Dykstra, 2012), where internal tides resuspend, rework, and deposit sediment across the canyon floor. Similarly, the starved ripples support reworking from a waxing tidal cycle before the deposition of mud drapes as the cycle wanes (Dykstra, 2012). The thick-thin cyclicity of couplets is shown to be genetically unique to internal tide deposits (Archer, 1996; Dykstra, 2012), supporting tidally forced processes, with the thicker banded couplets forming during stronger spring tides and thinner laminae couplets during weaker neap tides. Differentiating the deposits of internal tide reworking from the deposits of other deep ocean currents such as transitional flows is not trivial and requires close examination of sedimentary structures and full consideration of their paleogeographic context. This is examined further in the Discussion section (see the Interpretation of Internal Tide Deposits from the Ancient Rock Record section).

Mass-Transport Deposits (MTDs)

Description

Mass-transport deposits (MTDs) are between 1 m and 15 m thick and comprise a range of characteristics. Chaotic units comprise granule- to pebble-sized mudstone clasts supported by a poorly sorted sandstone-mudstone matrix. They lack grading and sedimentary structures and have irregular, erosional lower and upper boundaries (Fig. 3C). Deformed units range from tightly folded to overturned heterolithic packages to rotated thin-bedded heterolithic packages with minor internal deformation. MTDs either are laterally continuous across the overbank or form thick localized packages at areas close to the canyon margin.

Interpretation

The tightly folded and tilted heterolithic packages are interpreted as slump and slide deposits that record remobilized stratigraphy that formed positive relief (Pickering and Corregidor, 2005). The chaotic and poorly sorted matrix-supported units are interpreted as debrites deposited en masse under laminar flow conditions by cohesive debris flows (sensu Talling et al., 2012). The

irregular, erosive bases and top surfaces suggest high-energy scouring and entrainment of underlying substrate, which likely created rugose erosional relief on the canyon floor.

DEPOSITIONAL STAGES

The thin-bedded heterolithic stratigraphy of the canyon-confined overbank (FA3) is subdivided into a lower (stage 1) and upper (stage 2) succession (Fig. 3). The stages are distinguished by differences in the proportion and distribution of bed types, sand-to-mud ratio, bed thickness, grain size, paleoflow direction, and depositional architecture. These differences are summarized in Figure 7 and Table 2.

Stage 1 (Lower Overbank)

Stage 1 (10–18 m thick) represents the lower overbank (Fig. 3) and comprises packages of interbedded LDTCDs, minor TFDs, and mudstones, which are interrupted by thicker bedded HDTCDs and MTDs (Fig. 8). Stage 1 packages conformably overlie canyon axis deposits (Fig. 9) and contain a substantial proportion of sandstone (sand-to-mud ratio of 50:50; Table 2), with variable bed thicknesses (0.5–98 cm; Table 2). Stage 1 deposits also exhibit a wide grain-size distribution (medium silt to granule), with a tendency toward coarser grain sizes when compared to stage 2 (Fig. 7B). Paleocurrent directions obtained from ripples are generally toward the south-southeast, though a wide range of directions are documented in areas close to the canyon margin (Fig. 2A). The proportion of bed types varies little between areas close to channel elements and areas close to the canyon margin (Fig. 7C).

LDTCD beds compose ~20% of the total measured thickness of stage 1 (Fig. 7C). LDTCD 1 beds are thin (<10 cm thick), laterally continuous, and evenly distributed across the lower overbank with little lateral variation in sand-to-mud ratio (Fig. 7). LDTCD 2 beds are more clustered, forming thicker beds (10–20 cm thick), which thin upward from the base of the lower overbank, above laterally stacked channel elements (Fig. 8). They also cluster above HDTCD 2 beds near the canyon margin at the eastern edge of the overbank (Fig. 10). These beds commonly exhibit a wide range of paleocurrent directions, especially within packages close to the canyon wall (Fig. 10). TFDs compose ~10% of the total measured thickness of stage 1 (Fig. 7C), and TFD 1 and 3 beds are clustered toward the top of stage 1 while TFD 2 beds are typically clustered above MTDs and scour surfaces (Fig. 8). ITDs are rarely observed in stage 1.

HDTCDs compose ~29% of the total measured thickness of stage 1. They form discrete, outsized beds that are either laterally continuous for hundreds of meters with only minor changes in bed thickness (Fig. 9) or otherwise form isolated, highly bioturbated lenses, which pinch out laterally over tens of meters (Fig. 8C). HDTCD 1 beds are common near adjacent channel margin deposits on the western side of the lower overbank, where they are typically tabular with erosional bases and pebble lags (Fig. 9E). With increasing lateral distance away from channel elements, they gradually become less erosional and increasingly resemble hummock-like HDTCD 2 beds at locations within 10–20 m of the canyon margin (Fig. 10B). HDTCD beds pinch out abruptly at the canyon margin boundary.

Locally, thinner-bedded packages between HDTCD beds are disrupted by MTDs (~11% of the total measured thickness of stage 1). These mostly occur as mud-rich debrites, which are 4–5 m thick near canyon margins (Fig. 10D) but thin to form discontinuous lenses toward the canyon axis. Debrites either are observed near slumped packages of tightly folded and locally overturned LDTCD beds near the canyon margin (Fig. 10D) or otherwise underlie laterally

TABLE 2. THICKNESS, NUMBER OF BEDS MEASURED, SANDSTONE BED THICKNESS MEAN AVERAGE, RANGE, AND STANDARD DEVIATION, AND SAND-TO-MUD RATIO FROM PROXIMAL AND DISTAL AREAS OF THE CONFINED OVERBANK DEPOSITIONAL STAGES

Depositional stage	Proximal or distal to channel elements	Thickness	No. of beds measured (no. of sandstone beds)	Mean average, range, and standard deviation (StDev.) of sandstone bed thickness	Average sand-to-mud ratio
Stage 1: Lower overbank	Proximal	10 m	590 (296)	Average = 5.7 cm Range = 0.5–98 cm StDev. = 12 cm	50:50
	Distal	7 m	297 (148)	Average = 8.1 cm Range = 1–50 cm StDev. = 9.6 cm	50:50
Stage 2: Upper overbank	Proximal	28 m	901 (449)	Average = 2.6 cm Range = 0.2–30 cm StDev. = 5.1 cm	41:59
	Distal	12 m	239 (120)	Average = 1.6 cm Range = 0.1–15 cm StDev. = 2.5 cm	30:70

Note: Data are compiled from 2027 beds measured across the Punta Baja confined overbank (facies association 3 [FA3]). StDev.—standard deviation.

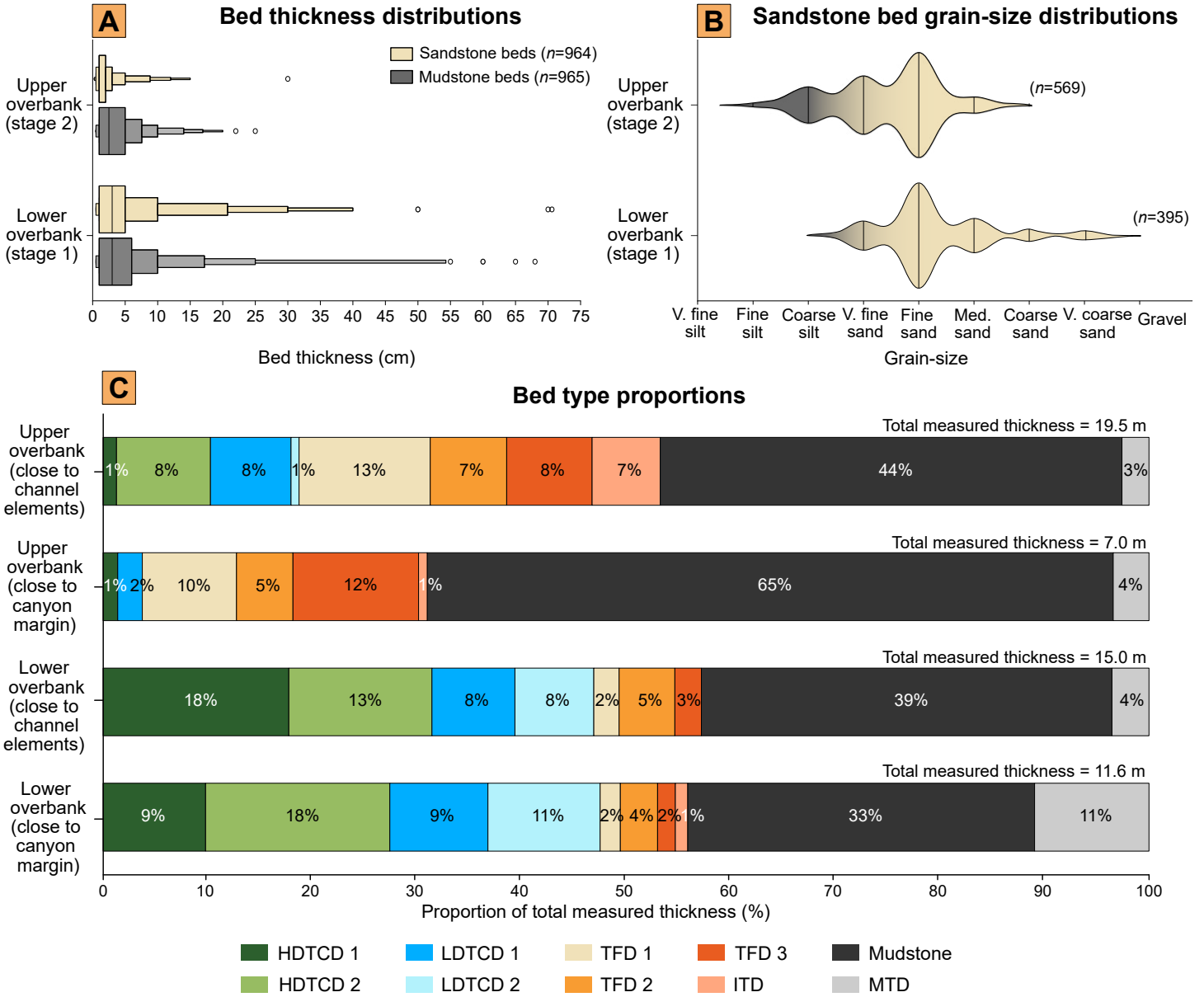

Figure 7. (A) Box plot showing distribution of sandstone and mudstone beds from upper and lower confined overbank. (B) Violin plot showing median grain-size distribution of sandstone beds from upper and lower confined overbank. (C) Bar plot showing proportions of different bed types by total measured stratigraphic thickness of upper and lower confined overbank. HDTCD—high-density turbidity current deposit; LDTCD—low-density turbidity current deposit; TFD—transitional flow deposit; ITD—internal tide-reworked deposit; MTD—mass-transport deposit.

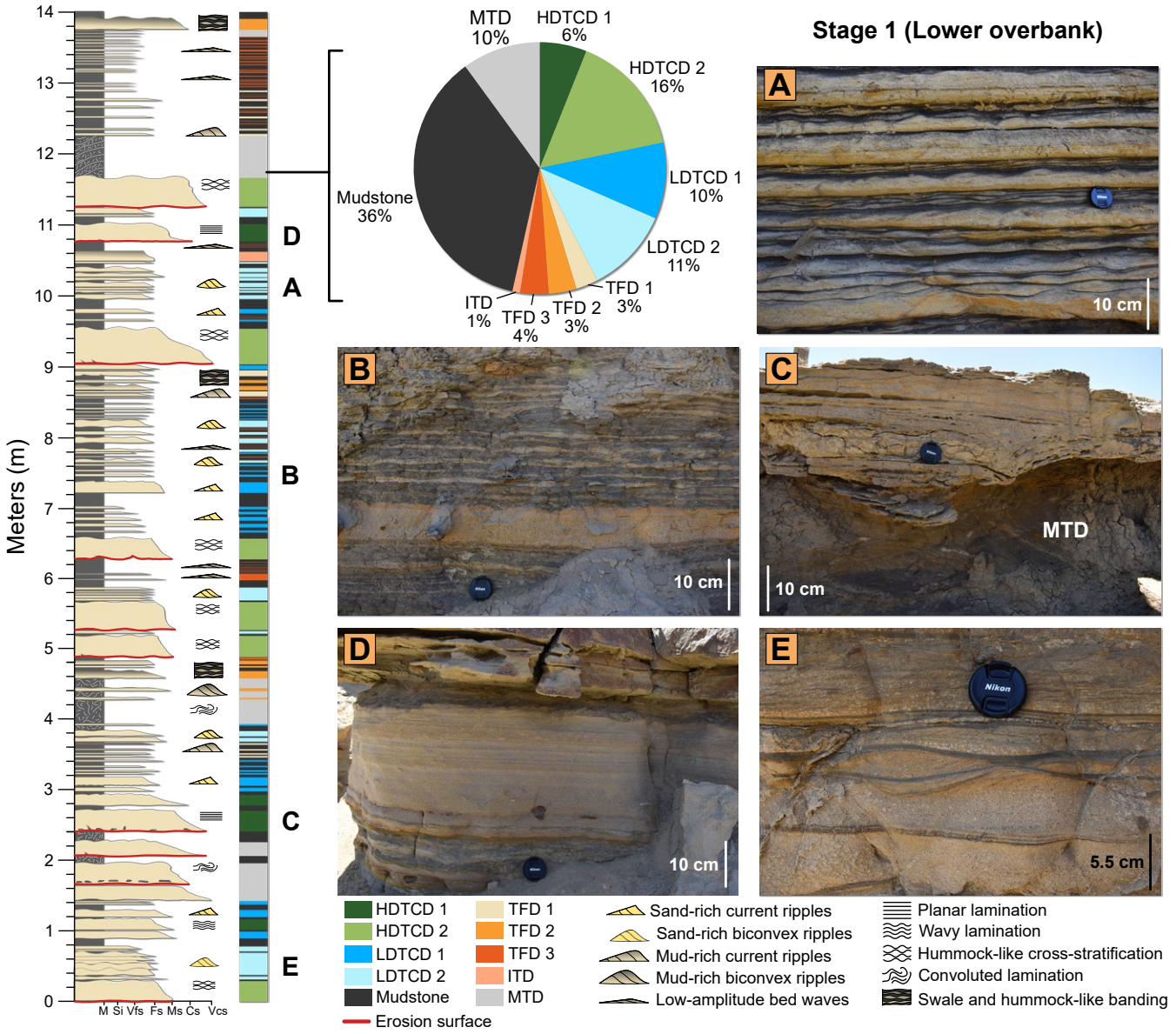

Figure 8. Composite log, bed type proportions, and representative photographs through lower confined overbank section (stage 1). (A) LDTCD 2 beds with structureless and biconvex ripple divisions. (B) Structureless LDTCD 1 bed which passes into sand-rich starved ripples. (C) HDTCD 1 bed thickening into a MTD. (D) HDTCD 1 bed with lower structureless and upper planar laminated divisions. (E) LDTCD 2 beds containing sand-rich biconvex ripples. HDTCD—high-density turbidity current deposit; LDTCD—low-density turbidity current deposit; TFD—transitional flow deposit; ITD—internal tide-reworked deposit; MTD—mass-transport deposit; M—mud; Si—silt; Vfs—very-fine sand; Fs—fine sand; Ms—medium sand; Cs—coarse sand; Vcs—very-coarse sand.

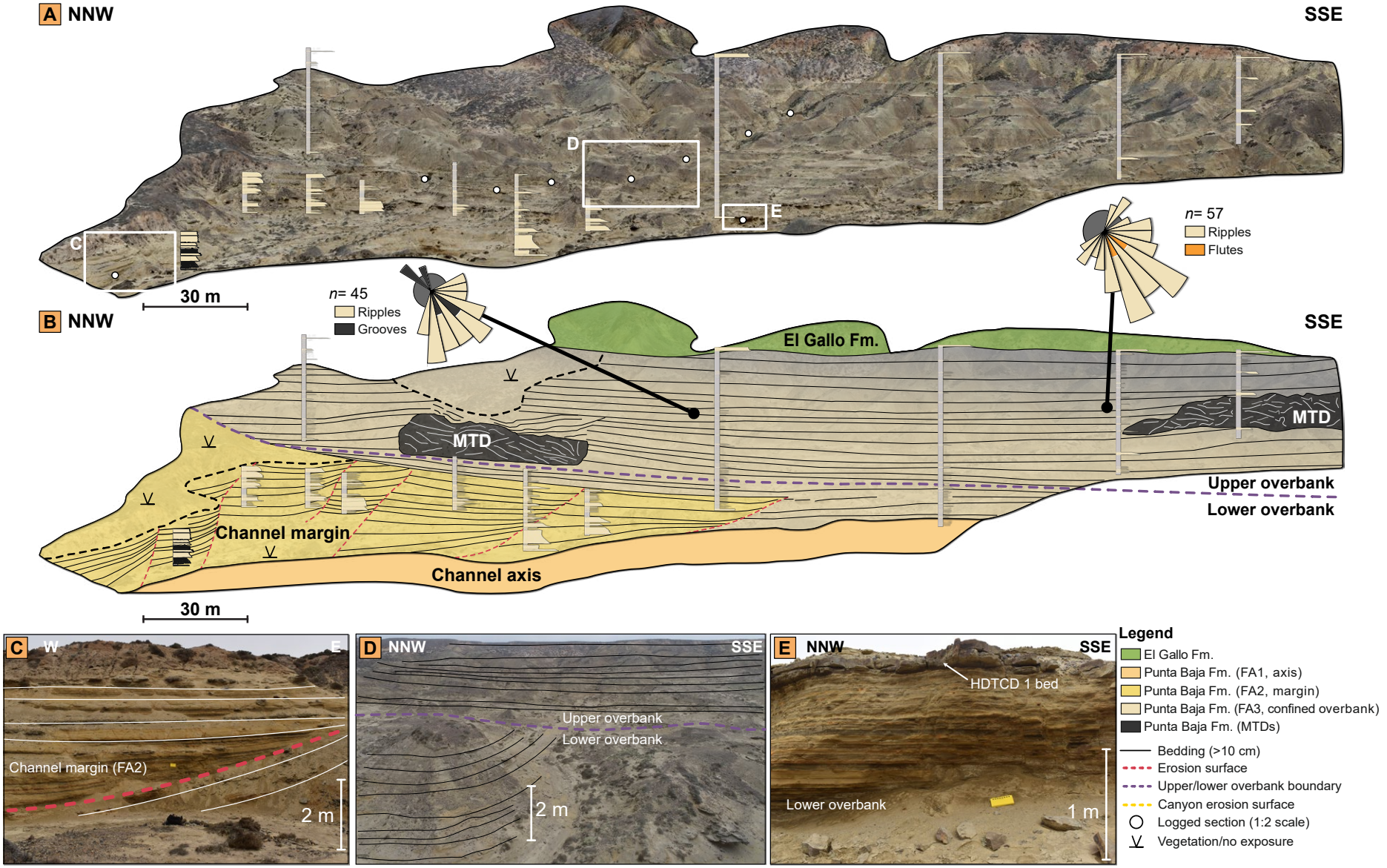

Figure 9. (A) Uncrewed aerial vehicle (UAV)–captured photogrammetric model of channel margin and lower and upper confined overbank packages of Punta Baja canyon fill, with sedimentary logs projected onto model. (B) Correlation panel of margin and confined overbank packages, with drawn interpretations of constituent beds, highlighting their lateral and stratigraphic variability. (C) Photograph of medium- to thick-bedded sandstone packages interpreted as channel margin deposit. (D) Photograph of confined overbank showing differences in bed thickness and grain size between lower and upper overbank stages. (E) Photograph of thin-bedded lower overbank package overlain by laterally continuous HDTCD 1 marker bed. Panel location is shown in Figure 2C. Rose diagrams are oriented with respect to panel. HDTCD—high-density turbidity current deposit; MTD—mass-transport deposit; FA—facies association.

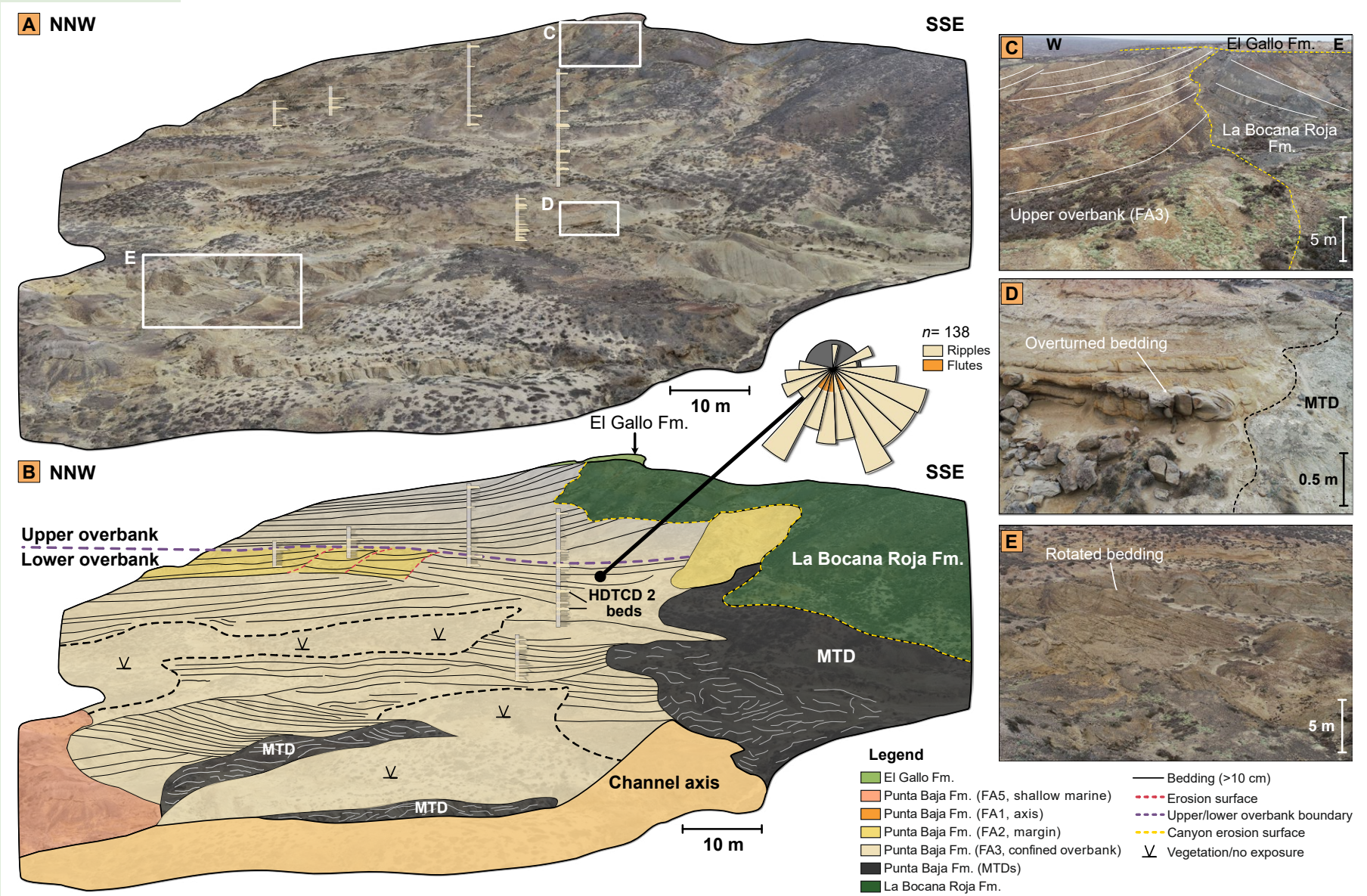

Figure 10. (A) Uncrewed aerial vehicle (UAV)–captured photogrammetric model of lower and upper overbank confined packages of Punta Baja Formation near canyon margin, with sedimentary logs projected onto model. (B) Correlation panel of confined overbank section, with drawn interpretations of main package types, highlighting lateral and stratigraphic variability of their constituent beds and their interactions with canyon wall. (C) Photograph of upper overbank packages onlapping onto canyon wall (La Bocana Roja Formation) and planed off by overlying El Gallo Formation. (D) Photograph of beds within lower overbank packages. Beds have been overturned with proximity to mass-transport deposits (MTDs), which were caused by canyon margin failure. (E) Photograph of lower overbank thin-bedded packages, which have been rotated due to lateral migration of channel axis. Panel location is shown in Figure 2C. Rose diagrams are orientated with respect to panel. HDTCD—high- density turbidity current deposit; FA—facies association.

discontinuous and wedge-shaped HDTCD beds (Fig. 8C). Slides are common at locations close to channel elements and comprise rotated packages of LDTCD beds that dip away from the canyon axis and lack internal deformation or disaggregation (Fig. 10E).

Stage 2 (Upper Overbank)

Stage 2 (20–50 m thick) represents the upper overbank (Fig. 3) and is marked by changes in bed type proportions compared to stage 1; TFDs are more common, with fewer HDTCDs and LDTCDs (Fig. 11). Thin-bedded packages of LDTCDs and TFDs between HDTCD beds have distinct fining- and thinning-upward trends (Fig. 11) and decay in thickness and grain size eastward toward the canyon margin (Fig. 10). Stage 2 is more mud prone than stage 1 (Table 2; sand-to-mud ratio of 41:59). Sandstone beds are thinner (2.6 cm thick on average), less variable in thickness (0.1–30 cm thick), and finer grained (Table 2). Overall, paleocurrent directions from ripples and grooves are toward the south, with a narrower range of directions and fewer examples of paleocurrent reversals than observed in stage 1 (Fig. 2A).

TFDs compose ~27% of the total measured thickness of stage 2, while turbidites (LDTCDs and HDTCDs) compose ~10% (Fig. 7C). TFD 1 beds are most common with an even stratigraphic distribution throughout stage 2, with some clustering of thicker beds near aggradationally stacked channel elements (Fig. 12). With lateral distance away from channel elements, the proportion of TFD 1 beds decreases, and beds gradually become thinner and muddier before transitioning into TFD 2 and 3 beds over ~100 m (Fig. 12). TFD 2 beds form discrete clusters across the upper overbank and become more widely dispersed in areas away from channel elements (Figs. 11 and 12). TFD 3 beds occur in thinner-bedded mud-rich packages, either interspersed between other TFD beds or isolated within thicker (1–2 m) mudstone packages (Fig. 11). The number and thickness of TFD 3 beds increase stratigraphically and laterally away from channel elements, and TFD 3 is the most common bed type at the canyon margin at the top of stage 2 (Fig. 12).

LDTCD beds compose ~7% of the total measured thickness of stage 2 (Fig. 7C). LDTCD 1 beds are clustered near the base of the upper overbank stage, near sand-rich channel margin deposits, while LDTCD 2 beds are rarely observed near sandier packages (Fig. 12). LDTCD beds transition into TFD 1 and 2 beds toward the canyon margin (Fig. 12).

HDTCDs compose ~8% of the total measured thickness of stage 2 and are evenly distributed but thin and fine stratigraphically and toward the canyon margin (Figs. 7C and 11). HDTCD 1 beds still occur as outsized, laterally continuous marker beds that truncate thin-bedded packages but are typically thinner and less erosional than HDTCD beds in stage 1 (Fig. 9). HDTCD 2 beds are rare and are clustered at the base of stage 2. MTDs are rare (~3%) and commonly occur as slides, where thin-bedded TFD packages are rotated toward the canyon margin, or as debrites, which occur as thin, laterally discontinuous intervals that extend across the upper overbank. ITDs (~7%) were observed on the western side of the canyon fill, intercalated with channel margin deposits and mud-rich, thin-bedded packages of stage 2 (Fig. 6).

DISCUSSION

A Model for the Evolution of Canyon-Confined Overbanks

An initial phase of incision and almost complete sediment bypass (Normark et al., 1993; Baztan et al., 2005; Stevenson et al., 2015), represented by the steep erosion surface and coarse-grained lag deposits in the canyon axis (Fig. 3), was followed by an aggradational stage, recorded by the overbank succession on the eastern margin of the canyon fill. This aggradation followed westward migration of channels and widening of the canyon fill, coupled with a decrease in the slope gradient from mass-transport deposition (Bouwmeester et al., 2025), which promoted the local onset of canyon aggradation and the development of canyon-confined overbank accommodation (Fig. 13A). As the canyon aggraded, sediment gravity flows in channels (FA1) were partially stripped and spilled into the overbank. Periods of axial erosion and entrenchment likely resulted in flow partitioning due to the elevation difference between the lower- and higher-density parts of stratified flows (e.g., Piper and Normark, 1983; Peakall et al., 2000; Keevil et al., 2006).

Lower Overbank (Stage 1)

The lower overbank (stage 1) records the early stages of canyon aggradation. The high sand-to-mud ratio, variable bed thicknesses, and wide grain-size distribution, with a higher maximum grain size than the upper overbank (Fig. 7; Table 2), suggest that the lower overbank received flows of varying magnitudes that were fully confined within the canyon. The lower overbank is therefore interpreted as a relatively high-energy environment where the dominant flow processes were fully turbulent sediment gravity flows (Figs. 13A and 13B). HDTCDs represent infrequent, higher-magnitude flows that overspilled adjacent channels to deposit medium-bedded turbidites, and LDTCDs represent lower-magnitude flows that deposited thin-bedded turbidites, where the dilute upper parts of flows were stripped and/or overspilled from channels into the confined overbank (Piper and Normark, 1983; Hiscott et al., 1997; Peakall et al., 2000; Hansen et al., 2015).

The consistent thickness and lateral continuity of most HDTCD beds suggest that higher-magnitude, fully turbulent flows were able to extend completely across the lower overbank and deflect and reflect against the canyon margin topography (Fig. 13B). The lateral transition from HDTCD 1 beds to HDTCD 2 beds within 10–20 m of the canyon margin, coupled with variable paleocurrent directions, supports an interpretation of flow transformation from a unidirectional flow to a combined flow, where upon incidence with the base of the canyon wall, flows decelerated rapidly, resulting in high rates of suspended

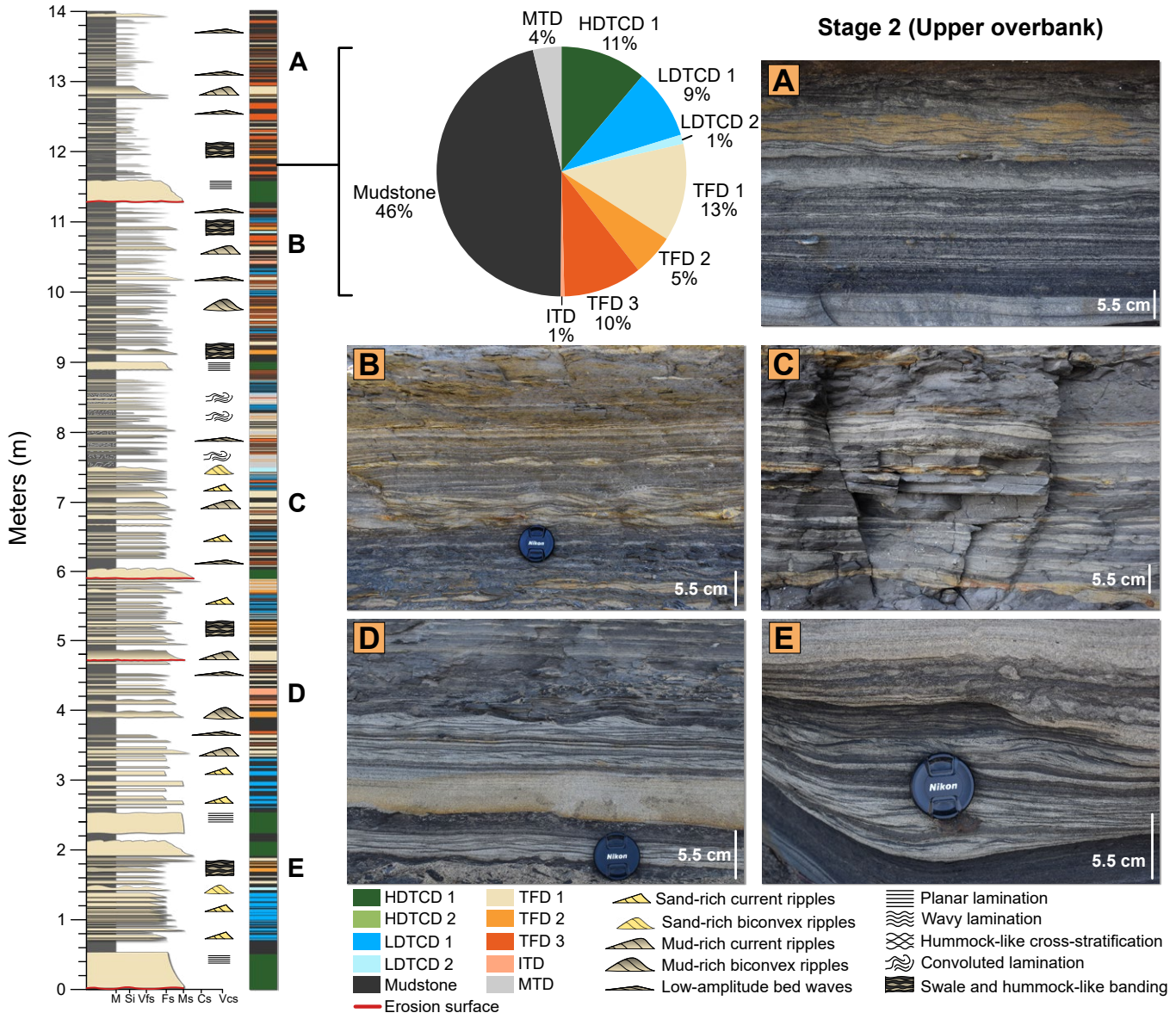

Figure 11. Composite log, bed type proportions, and representative photographs through upper confined overbank section (stage 2). (A) TFD 3 bed containing low-amplitude bed waves overlain by TFD 1 bed containing mud-rich current ripples. (B) TFD 1 beds comprising lower division of mud-rich current ripples before passing into division of longer, thinner low-amplitude bed waves and starved ripples. (C) TFD 1 beds with large mud-rich ripples. (D) ITD bed showing reworking of (sand-rich) sediment gravity flow deposit by internal tides, characterized by "rhythmic" thin-thick lamination and starved ripples. (E) TFD 2 beds, demonstrating sandstone-mudstone banded sets and mud-rich ripples. HDTCD—high-density turbidity current deposit; LDTCD—low-density turbidity current deposit; TFD—transitional flow deposit; ITD—internal tide-reworked deposit; MTD—mass-transport deposit; M—mud; Si—silt; Vfs—very-fine sand; Fs—fine sand; Ms—medium sand; Cs—coarse sand; Vcs—very-coarse sand.

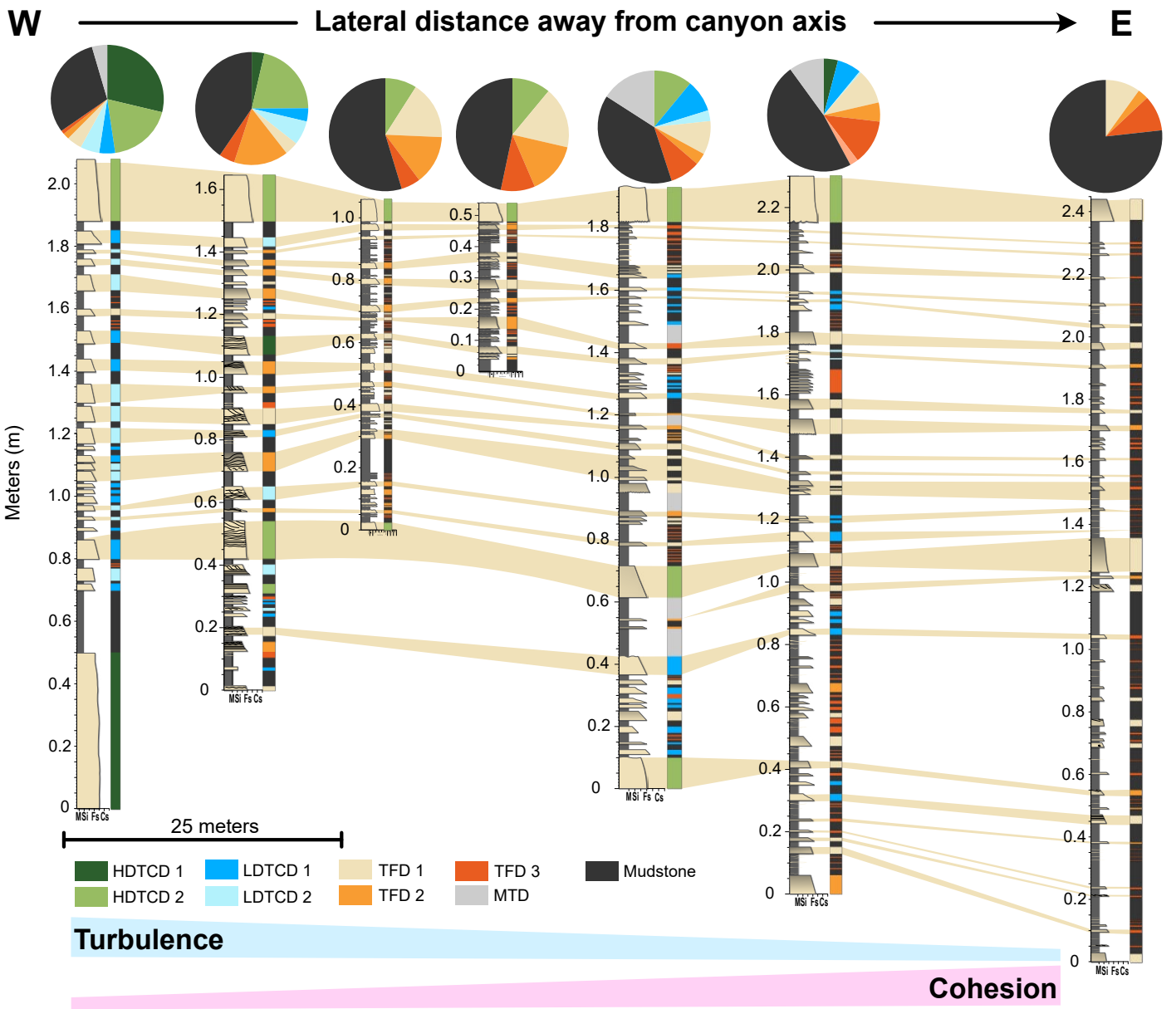

Figure 12. Bed-scale correlation panel of representative 2 m section from upper confined overbank highlighting across-strike distribution and lateral transitions of different bed types over a distance of 100–200 m. Location of panel is shown in Figure 2A. HDTCD—high-density turbidity current deposit; LDTCD—low-density turbidity current deposit; TFD—transitional flow deposit; MTD—mass-transport deposit; M—mud; Si—silt; Fs—fine sand; Cs—coarse sand.

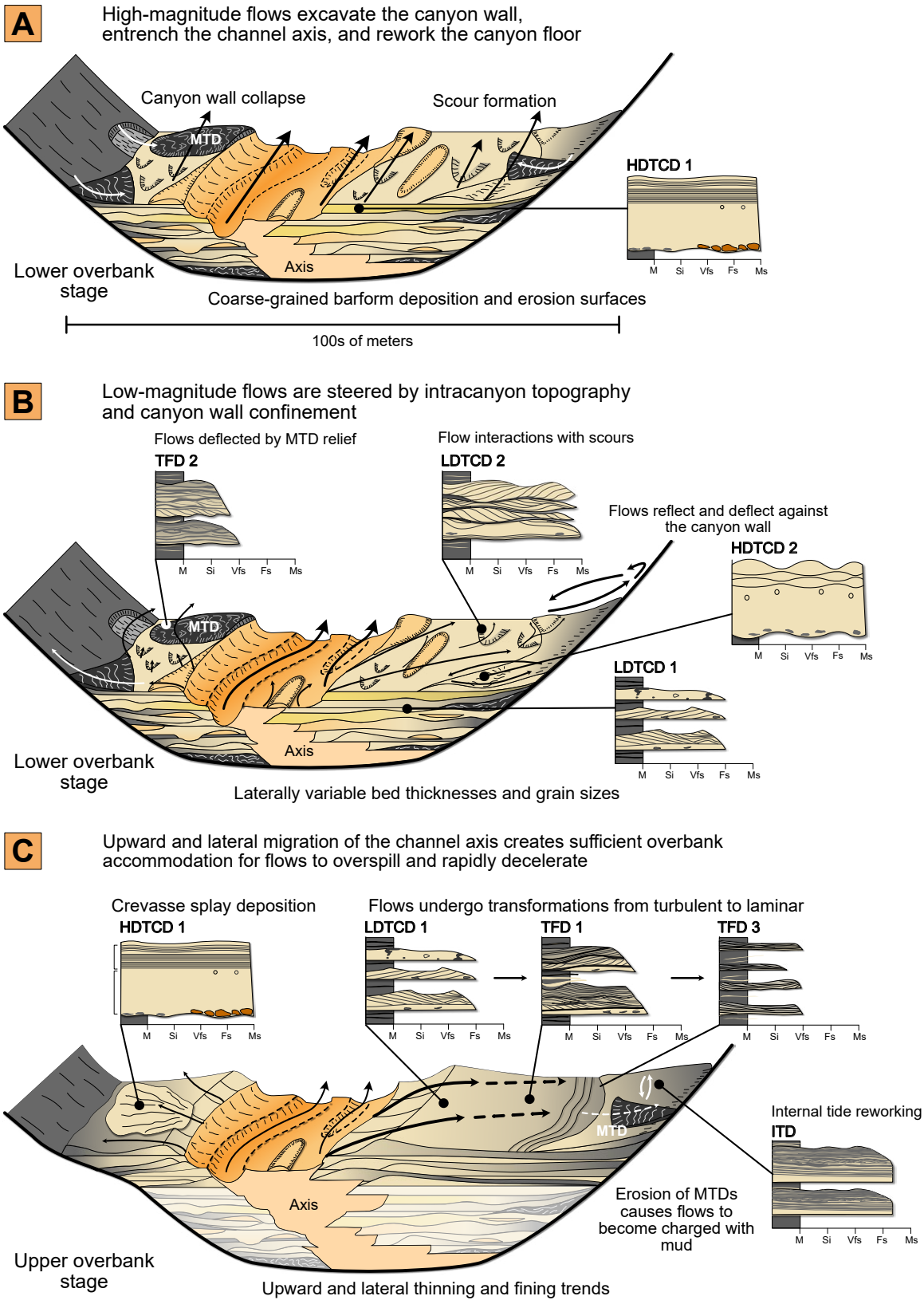

Figure 13. Conceptual diagram of a canyon setting, showing locations where different flow transformations and bed types are expected to form. (A) Lower overbank stage where high-magnitude, erosional flows are the dominant process. (B) Lower overbank stage where lower-magnitude flows are affected by complex canyon topography. (C) Upper overbank stage, where canyon widening creates sufficient accommodation for flows to overspill and transform between turbulent and laminar states. HDTCD—high-density turbidity current deposit; LDTCD—low-density turbidity current deposit; TFD—transitional flow deposit; ITD—internal tide-reworked deposit; MTD—mass-transport deposit; M—mud; Si—silt; Vfs—very-fine sand; Fs—fine sand; Ms—medium sand.

sediment fallout and the formation of thick, massive sandstone beds (HDTCD 2). The hummock-like bedforms at the tops of HDTCD 2 beds are attributed to interaction of deflected flows running perpendicular to the incoming depletive parental flow. These interactions generated a combined flow, likely in the absence of an oscillatory component (Keavney et al., 2025a; Wang et al., 2025), and reworked beds into dune-scale hummock-like bedforms. The abrupt pinch-out of HDTCD 2 beds at the base of the canyon wall surface (Fig. 10) suggests that some flows had limited upslope momentum and were unable to deposit onto the canyon wall (Keavney et al., 2025a). The lateral continuity and uniform thickness of some HDTCD beds suggest that after interacting with the canyon wall, returning flows may have been able to re-enter the channel, potentially facilitated by the steepness of the lateral slope (Abd El-Gawad et al., 2012). The clustering of LDTCD 2 beds is interpreted to record higher-momentum flows that were able to propagate farther up the canyon wall. Here, upon incidence with the base of the canyon wall, an incoming parental flow became stripped, generating thin, dilute multidirectional flows, which propagated onto the canyon wall surface and collapsed downward. These flows were then superimposed onto the initial parental flow, generating a combined flow that reworked beds into sand-rich biconvex ripples, as observed in LDTCD 2 deposits. The even stratigraphic distribution of HDTCD 2 and LDTCD 2 beds near the canyon margin (Fig. 8) suggests that combined flows were repeatedly generated from reflection and deflection against the canyon wall. This supports an interpretation that the lower overbank was highly confined by steep canyon walls. The variable paleocurrent directions and flow reversals near the canyon margin (Fig. 2A) demonstrate flow complexity on incidence with the canyon wall (Soutter et al., 2021). Mechanisms to generate this flow complexity include a rugose canyon margin surface or that flows were stripped or overspilled from different parts of evolving channel bends, resulting in a range of flow incidence angles with the canyon wall (e.g., Tek et al., 2022; Wang et al., 2025).

LDTCD 2 beds nearer the channel axis (Fig. 7C) point to seabed topography in the overbank. Lower-magnitude flows likely reflected and deflected against evolving erosional and depositional relief formed by scour surfaces and MTD topography to set up combined-oscillatory flows (Fig. 13). Scour surfaces were likely formed by erosive, higher-magnitude flows that incised and entrained overbank deposits, while MTDs were sourced from canyon flank collapse (Fig. 10). This resulted in mud-rich debrites that extended across the overbank, forming complex relief.

The discontinuous wedge-shaped HDTCD beds above MTDs are interpreted as partially confined deposition from strongly bypassing high-magnitude flows. Clusters of TFD 2 beds above MTDs are records of combined transitional flows that became increasingly cohesive through mud entrainment and deflection against MTD relief. Slumps and slides near channel elements likely represent collapse of thin-bedded packages from undercutting of the overbank by channel migration (Boehlke and Abbott, 1986). Furthermore, the observation of LDTCD 2 beds at the base of the lower overbank points to flow interactions with topography resulting from the westward lateral-oblique migration of channel elements during the initial stages of overbank aggradation. Upward transitions from combined flow beds (LDTCD 2 and HDTCD 2) to LDTCD 1 beds (Fig. 8) support gradual healing of the overbank relief with lower-magnitude turbulent flows able to traverse the overbank with minimal topographic influence.

The general paucity of TFDs across the lower overbank, apart from those overlying mud-rich MTDs, is likely due to limited mud-rich substrate available for entrainment. The initial substrate would have comprised conglomeratic and sand-rich channel elements, and later, sand-rich HDTCD beds (Boehlke and Abbott, 1986; Kane et al., 2022). Furthermore, the strongly confined setting of the lower overbank and thus shorter lateral distances to the canyon margin would have caused flows to decelerate too quickly before interacting with the canyon wall, thereby inhibiting transformations from turbulent to laminar flows.

Upper Overbank (Stage 2)

The transition to the upper overbank (stage 2) is marked by an increase in the proportion of TFDs and a notable decrease in the thickness and number of HDTCDs over a stratigraphic thickness of ~10 m (Figs. 9 and 10). The lower sand-to-mud ratio, thinner and less variable bed thicknesses, and a narrower grain-size distribution with an overall lower maximum grain size (Fig. 7) suggest that the upper overbank received smaller-magnitude flows than the lower overbank, supporting an interpretation of an overall lower-energy and more stable depositional environment (Fig. 13C). Transitional flows were more common than cohesionless, turbulent flows (Fig. 11), demonstrating that the upper overbank was conducive to flow transformations. The observation of TFDs in the canyon-confined overbank described here further indicates that transitional flow behavior is not solely restricted to distal submarine settings, such as lobe fringes (e.g., Baker and Baas, 2020). TFDs can instead be used across a broad range of submarine settings to indicate sites of erosion into mud-rich substrates and abrupt losses in confinement, where flows are forced to decelerate (Taylor et al., 2024).

TFD 1 beds represent unidirectional flow transformation from an initially turbulent flow to a turbulence-modulated transitional flow. Their even distribution near channel elements demonstrates that flows experienced abrupt decreases in confinement as upper parts of flows were stripped or overspilled channels and decelerated rapidly (Peakall et al., 2000; Hansen et al., 2015). The higher preservation of channel margin deposits in the upper stage (Fig. 9) suggests a higher channel sinuosity and therefore more abrupt losses in confinement from overspill. Given this, transitions from turbulent to transitional flows were possibly enhanced by stronger flow partitioning, where dilute upper parts of overspilling flows became relatively more enriched in mud as the denser sand-rich fraction of flows remained channel confined. Ultimately this would result in increased cohesive forces in decelerating flows, promoting turbulence modulation and the generation of mixed-grain-size bedforms. Further increases in cohesion may have been driven by the entrainment of fine-grained, sand-rich substrate at channel margin areas (Baker and Baas, 2023). For high-density,

strongly cohesive sediment gravity flows dominated by transitional or laminar flow behavior, the addition of a small amount of noncohesive sediment is expected to further increase the cohesive strength of the plug layer and instigate further decreases in flow mobility (Baker and Baas, 2023).

More mud or very fine sand was likely deposited and preserved in the upper overbank compared to the lower overbank where mud was more likely bypassed or resuspended by high-magnitude flows. Additional mud-rich substrate was likely derived from collapse of unstable canyon walls and emplacement of debris flows. The upward and lateral transitions from sand-rich turbidites (LDTCD 1 beds) to TFDs near channel elements indicate the initial phase of transformation from fully turbulent, noncohesive flows to transitional flow conditions.

The transition from TFD 1 beds through TFD 2 to TFD 3 beds with distance from channel elements (Fig. 12) points to lateral flow transformations from lower transitional plug flow to upper transitional plug flow conditions as flows escaped channel confinement and decelerated but remained within the confines of the canyon. The transition from TFD 1 to TFD 3 beds over 100–200 m demonstrate particularly rapid flow transformations. The rate of flow transformation with distance is more rapid than those recorded for other depositional environments in previous studies, such as internal levees in mid-slope settings, where flows transform over 1–2 km (Taylor et al., 2024), and distal lobe fringe environments, where flows transform over 2–3 km (Baker and Baas, 2020).

The distinct clusters of TFD 2 beds in the upper overbank (Fig. 12) suggest that some flows were susceptible to topographic influence as they decelerated and thinned (Kneller and Buckee, 2000). Here, TFD 2 beds are interpreted where flows transitioned over mud-prone substrates and interacted with subtle seabed topography, such as scour surfaces or mud-rich debrite relief (Pope et al., 2022). Mudstone caps suggest deposition in topographic lows (Pickering and Hiscott, 1985; Haughton, 1994). In areas close to the canyon margin, clusters of TFD 2 beds imply that some decelerated transitional flows were just about able to reflect and deflect off the canyon walls.

The high proportion of TFD 3 beds in parts of the upper overbank near the canyon margin (away from channel elements) represents the lateral extent of overspilling unidirectional transitional flows (Fig. 12). The upward increase in TFD 3 beds with respect to TFD 1 and 2 beds suggests a higher number of unidirectional flows that were able to overspill and fully decelerate across the overbank. This can be attributed to a combination of increased channel relief with time (Hiscott et al., 1997; Pirmez and Imran, 2003), a wider overbank area (Maier et al., 2012; Hansen et al., 2015), and a decrease in the magnitude of sediment gravity flows as the system aggraded (Kneller, 2003).

The rarer occurrence of HDTCDs in the upper overbank compared to the lower overbank implies that higher-magnitude flows were either less frequent or increasingly confined to channels within the canyon conduit. Packages of tabular HDTCD 1 beds thin with lateral distance from channel elements and pinch out abruptly, suggesting breaching of channel confinement, most likely at the outer bend of the channel (Lowe et al., 2019). ITDs were almost exclusively observed in the upper overbank (Figs. 11D and 11E). This is likely because the upper overbank was a lower-energy environment, with an availability of sand from overspilling low-magnitude flows to rework into ITDs. The decrease in HDTCDs point to increased ITD preservation potential in the upper overbank section, given that frequent high-magnitude flows would remove ITDs.

The differences documented between the lower and upper overbank stages can be attributed to the interplay of several factors. In part, the changes in sedimentary processes record the response to the widening of the canyon during aggradation (Fig. 13). As the narrow, steeply confined lower part of the canyon aggraded, the overbank widened, which increased the accommodation for flows to spread across. This change was exacerbated by a decrease in the rugosity of seafloor relief due to fewer canyon margin landslides and gradual healing of the overbank relief. Therefore, as the canyon-confined overbank widened during aggradation, it also became increasingly mud rich and smoother, supporting conditions for flow transformations (Fig. 13C). These changes promoted the increased proportion of TFDs and decrease in the thickness and number of HDTCDs. Another factor might have been an increase in the relief between the thalweg of active channels in the axis and the overbank, which would inhibit the magnitude of overspilling flows. However, the instantaneous relief between the thalweg and overbank surface is hard to constrain from the rock record. In the cases of both channel widening and changes in relief and thus overspill, a progressive transition in sedimentation might be expected, yet while locally gradational, the changes between the lower and upper overbank stages are abrupt, largely taking place over a few meters (Figs. 9 and 10). This abrupt change suggests that there may have been additional processes driven by external forcing.

Basinward tilting and faulting controlled the juxtaposition of continental and marine sedimentary systems (Busby et al., 1998) and the orientation of the canyon (Kane et al., 2022), respectively. Therefore, the role of tectonics on the abrupt change between the lower and upper overbank successions should be considered. Basinward tilting of this tectonically active margin may have influenced canyon initiation and erosion and could thus have caused an abrupt decrease in gradient to drive canyon aggradation. Repeated cycles of slope degradation and progradation have been identified in Mesozoic submarine canyons offshore Norway (Jackson et al., 2021), where basinward tilting was identified as the main driver and the position of the pivot point as the key control on the nature of the canyon fill. Such a process might be expected to lead to an abrupt change in depositional style. Other external changes such as increases in mud supply and/or a narrower range of flow magnitudes as the supply system matured may have occurred; however, they are perhaps harder to link to the abrupt changes in sedimentation, in marked contrast to the known abrupt changes in tectonics in this canyon system (e.g., Busby et al., 1998).

The Dynamic Nature of Canyon-Confined Overbank Successions

The variety of bed types and their complex distributions described here demonstrate that the Punta Baja canyon-confined overbank was a highly

dynamic environment. The heterogenous overbank succession records a diverse range of flow types, transformations, and complex interactions with topography that evolved through time. Therefore, interpretations of canyon-confined overbank successions require consideration of individual flows and their three-dimensional interactions with topography and not only assessment of depositional environment.

Comparisons with Models of Confined Overbank Sedimentation

Currently, models that describe confined overbank successions are derived from channel-levee systems from mid- to lower slope settings. They describe terrace deposits (Hansen et al., 2015, 2017) and internal levee deposits (Babonneau et al., 2004; Dykstra and Kneller, 2009; Kane et al., 2009; Kane and Hodgson, 2011; Morris et al., 2016; McArthur et al., 2020), which are distinguished by their external morphology and internal sedimentological characteristics (Hansen et al., 2015). Terrace deposits are defined as flat-lying, sheet-like deposits formed by turbulent flows that overspill channels, extend across the entire conduit, and reflect and deflect against confining surfaces (Hansen et al., 2015). Internally, they comprise packages of thin-bedded turbidites with variable bed thicknesses that show minimal lateral variation in sandstone proportion with distance away from channel elements (Hein and Walker, 1982; Schwarz and Arnott, 2007; Hansen et al., 2017). Conversely, internal levee deposits are wedge-shaped features that, unlike terrace deposits, form when there is sufficient space within the conduit for flows to overspill, decelerate, and deposit most of the suspended sediment before reaching the confining surface (Hansen et al., 2015, 2017). When compared to terrace deposits, internal levees have less variable bed thicknesses within thin-bedded packages and exhibit fining- and thinning-upward trends (Beaubouef, 2004; Kane et al., 2009; Kane and Hodgson, 2011).

The lower overbank stage documented here potentially acts like a terrace deposit, with the terrace surface formed by the oblique upward migration of channels (Babonneau et al., 2010; Maier et al., 2012). The confined nature of the bounding surface meant that flows were able to reflect and deflect against the canyon wall. Similarly, the upper overbank stage meets some of the criteria for internal levees, with discrete thin-bedded packages that fine and thin upward and laterally toward the canyon margin (Fig. 13C). However, these environmental models of confined overbanks only invoke stable flow conditions, such as waning turbulent flow processes in an otherwise dynamic environment where flow transformations are common (Fig. 13). Furthermore, they only consider lateral changes from channel element to master confining surface and do not fully consider the 3-D shape and distribution of beds and packages of beds. While there may be a general trend from a more terrace deposit–like stage to a more internal levee–like stage as the canyon is filled, this bimodal environment setting approach obscures three-dimensional variability that comes from evolving erosional and depositional topography within canyons.

Canyon-confined overbanks are highly dynamic environments with a wide range of erosional and depositional bedforms and MTDs, which generate complex and dynamic relief (Fig. 13). The evolving position and form of the channels within the canyon result in a wide range of flow types and deposits in the overbank, which limits the development of discrete architectural elements. Therefore, end-member models for confined overbank environments in submarine canyons are too simplistic. A criterion proposed for differentiating thin-bedded depositional environments has been to use the standard deviation of sandstone bed thicknesses and sandstone proportions (Hansen et al., 2017, their fig. 15). However, values of the standard deviation of bed thickness (1.3–26.7 cm) and sandstone proportion (18.8%–51.8%) from the Punta Baja confined overbank spans all fields of terrace deposits, internal levee, and external levee (Hansen et al., 2017), showing that canyon-confined overbanks are too dynamic to attribute to a single depositional environment.

Comparisons with Modern Canyon Terraces

Canyons pose a particular challenge in the long-standing endeavor of improving understanding of deep-water sedimentology by integrating observations of processes and products in modern and ancient systems (Mutti and Normark, 1987). In part, this is due to the destructive power of flows monitored in modern canyon systems (e.g., Pope et al., 2022). However, Fildani (2017) pointed out that the disparity in time scales between sediment entering a canyon head and its eventual transport to the deep-sea fan implies that submarine canyons may accumulate sediment over 10^3–10^5 years and discharge them during infrequent, high-magnitude "flushing" events (Paull et al., 2005). Geophysical surveys reveal extensive terrace features in canyon-proximal locations (Babonneau et al., 2010; Maier et al., 2018), which serve as ideal locations for sediment storage. Nonetheless, the interpretation of sedimentary processes in modern submarine canyon systems is hindered by the paucity of sedimentological successions preserved or intersected in these highly erosional systems (e.g., Babonneau et al., 2004; Arzola et al., 2008; Li and Clift, 2023). Therefore, the high-resolution stratigraphic framework developed here can help reveal the dynamic complexity of canyon terrace deposits at scales finer than those collected from modern canyons.

At the larger geomorphological scale, modern canyon terraces display a range of characteristics that correspond to their evolutionary phase (e.g., de Almeida et al., 2015). Two broad types of terrace surfaces are observed. Lower-elevation terraces are typically narrow and discontinuous features (Arzola et al., 2008; Guiastrennec-Faugas et al., 2020; Cerrillo-Escoriza et al., 2024). They are characterized by a combination of large-scale depositional relief from canyon-flank landslides (Paull et al., 2013; Pope et al., 2022; Ruffell et al., 2024) and erosional bedforms, such as scours, formed by high-magnitude bypassing flows (Li et al., 2020). Conversely, more elevated terraces tend to be wider and more continuous (Babonneau et al., 2002; Smith et al., 2005; de Almeida et al., 2015; Guiastrennec-Faugas et al., 2020; Cerrillo-Escoriza et

al., 2024). Their surfaces also tend to be smoother and less rugose and lack debris aprons (Paull et al., 2013). Generally, they dip laterally away from the canyon axis (Maier et al., 2018).

The lower overbank stage documented in the Punta Baja Formation shares affinities with the lower, steeply confined, narrow terraces in modern systems due to variable bed thicknesses, a wide grain-size range, laterally continuous landslides, scour surfaces, and combined flow beds (HDTCD 2 and LDTCD 2 beds). These observations suggest that flows that overspill onto modern terraces would likely be disrupted by seabed topography and reflect and deflect against the canyon wall across a relatively narrow terrace surface. The lower relief between the channel and terrace surface would promote a wide range of grain sizes and bed thicknesses due to limited flow partitioning. Similarly, the upper overbank stage may correspond with more elevated modern canyon terraces due to the increased proportion of TFD beds, which indicate that overspilling flows underwent flow transformations from turbulent to laminar. In modern elevated terraces, flow transformations would have been promoted by the smoother and wider terrace surfaces to allow mud-rich flows to run out and decelerate. TFDs are more likely observed in these settings due to the higher relief between channels and terraces, which promotes stronger flow partitioning, whereby the dilute upper parts of flows become increasingly enriched in mud relative to other grain-size components.

These observations are further supported at smaller scales by shallow piston cores from lower and upper terrace deposits from the Setúbal and Nazaré submarine canyons on the west Iberian margin (Arzola et al., 2008). Similar distributions of bed types are observed to the dataset presented here. In the lower, narrower terraces of the Nazaré Canyon, thick, sand-rich turbidites (which correspond to HDTCD 1 beds) are observed with variable bed thicknesses (Arzola et al., 2008, their fig. 5). These assemblages are accompanied by debrites with distorted fine sand layers above (Arzola et al., 2008, their fig. 17), which is comparable to the lower overbank of this study. Similarly, a core section from a low-terrace deposit in the Capbreton submarine canyon in Bay of Biscay, France (Guiastrennec-Faugas et al., 2020), reveals alternating layers of medium-grained sand and mud of varying thickness displaying ripple cross-lamination. These strata are interpreted as the result of low-energy gravity flows that were able to deposit coarser sediment onto the terrace (Guiastrennec-Faugas et al., 2020, their fig. 8). The deposits on wider elevated terraces of the Nazaré Canyon (Arzola et al., 2008) comprise thin-bedded, fine-grained turbidites with rare thicker, sand-rich beds deposited in an overall mud-rich setting. Alternating millimeter-scale sand-rich and mud-rich bands are observed (Arzola et al., 2008, their fig. 7), which might represent mixed-grain-size bedforms formed under transitional flows (Stevenson et al., 2020). Elevated terraces in the Upper Zaire Canyon (Babonneau et al., 2004, their fig. 14) display similar characteristics, including thin beds of structureless, very fine sand that pass into alternating thin laminae of clayey silt and very fine sand. These may also represent transitional flow conditions, which compares favorably with the deposits of the upper overbank documented in this study.

Existing models of terrace deposits and internal levee deposits are derived from channel-levee complexes from mid- to lower slope settings where flows construct external levees outside of the main confinement surface (e.g., Kane and Hodgson, 2011; Hansen et al., 2015). The ability of flows to overspill from the main confinement surface has the effect of filtering out the upper fine-grained component of flows, thus restricting the range of deposits that form within the conduit (Amos et al., 2010). In canyons, flows are fully confined by steep erosion surfaces with little to no external levee construction. Therefore, unfiltered flows within canyons are likely to be more variable and dynamic in their sedimentological characteristics than overbanks of more basinward channel-levee systems. Nonetheless, the stratigraphic changes in sedimentology documented here demonstrate the utility of confined overbanks as more complete records of submarine canyon evolution than adjacent canyon axes, which preserve a more complicated record of submarine canyon evolution, with the adjacent axis preserving a more complicated record of phases of bypass, accumulation, and flushing (Fildani, 2017). If discrete environments are labeled primarily based on their geometries, as in the case of terrace deposits and internal levees, then their efficacy as archives for paleoenvironmental change could be hindered. In summary, based on comparisons to existing confined overbank models and terraces in modern canyon systems, we infer that overbank environments confined within canyons must be assessed in relation to channel element stacking patterns, their three-dimensional nature, and their changes in paleoenvironment linked to the evolution of the system.

Interpretation of ITDs from the Ancient Rock Record

Internal tides have been shown to resuspend and transport sediment in submarine settings worldwide (Shepard and Marshall, 1969; Shepard, 1976; Gardner, 1989). However, their deposits have been rarely identified in the rock record (e.g., May and Warme, 2000; He et al., 2011). This may be due to an interpretive bias toward sediment gravity flow deposits in the rock record (Zhenzhong and Eriksson, 1991; Shanmugam, 2003; Dykstra, 2012) or their poor preservation potential given the erosive power of sediment gravity flows within canyon axes that may remove previous deposits (Maier et al., 2019; Talling et al., 2023). The interpretation of internal tide-reworked sands from the stratigraphic record has long been contested (e.g., Shanmugam and Wang, 2014). However, recent studies have successfully verified sedimentological observations from sediment traps and cores with direct measurements of internal tides from the Monterrey Canyon, California (Maier et al., 2019), and Logan Canyon, eastern Canada (Normandeau et al., 2024). Attempts can now be made to interpret ITDs from ancient canyon fills to support paleoenvironmental reconstructions. Observed modern ITDs comprise sharp-topped sandstones with abrupt grain-size breaks from sand to mud and planar or wavy silt and fine sand laminasets, which form thick-thin sand-mud couplets (rhythmites) with normal and inverse grading and mud-draped starved ripples (Maier et

al., 2019; Normandeau et al., 2024). Therefore, these studies can be used as recognition criteria to support interpretation of ITDs, characterized by waxing and waning tidally forced flows that resuspend and redistribute sediment on bed tops (Visser, 1980).

Most of the facies reported from modern systems as indicative of ITDs (apart from bidirectional ripples) are observed in the interpreted ITDs from the upper overbank (Fig. 7). This supports an interpretation that internal tides were present and strong enough to transport and rework sediment in the Punta Baja canyon. However, differentiating the deposits of internal tides from those of other processes that generate mixed-grain-size bedforms, such as transitional flows, is challenging. Observed similarities between ITDs and TFDs from the Punta Baja Formation include alternating sandstone-mudstone laminae and banded sets, and discontinuous starved laminae (Fig. 6). The cyclical laminae and banded couplets, with thick-thin transitions between "double bands", bear closer resemblance to deposits that were reworked by internal tides (Visser, 1980; Shanmugam, 2003). The interpreted ITDs here are not strongly aggradational, nor do they include high-angle climbing bedforms such as mud-rich current ripples (Fig. 6). This supports these deposits being the result of reworking of sediment gravity flow deposits by internal tides rather than TFDs. Furthermore, the absence of continuous transitions between different bedforms (i.e., from mud-rich current ripples to low-amplitude bed waves) in a single deposit also suggests that these deposits did not undergo flow transformations from turbulent to laminar (Fig. 6).

The proportion of observed ITDs in the Punta Baja canyon is low (~9% of total measured sections). The low abundance in other areas of the overbank is likely due to complete removal by higher-magnitude sediment gravity flows that overspilled into the overbank and/or to bioturbation that destroys laminae and banded sets (Li et al., 2019; Normandeau et al., 2024). In some ITDs observed in the Punta Baja overbank, the presence of thin, discontinuous laminae, coupled with a mottled texture above laminasets, might support reworking of sediment by organisms (Fig. 11D). Preservation potential of ITDs requires sedimentation rates that outpace the rate of bioturbation. Dykstra (2012) suggested that increased sediment availability could lead to higher preservation potential of ITDs. In canyons, storm events have been shown to increase suspended sediment concentrations (Li et al., 2019), which has been linked to increased preservation potential of ITDs (Yang et al., 2020). Another mechanism could be the influence of earthquake activity, given the tectonically active forearc basin setting, which would increase suspended sediment concentrations (Mountjoy et al., 2018). These events are likely contributing factors for the preservation of ITDs in the upper overbank of the Punta Baja canyon fill.

CONCLUSIONS

This study presents an exceptional example of an exhumed submarine canyon-confined overbank from the Upper Cretaceous Peninsular Ranges forearc, Mexico. Herein, we develop the first model of overbank sedimentation in ancient submarine canyons. The early stage of overbank sedimentation was dominated by turbulent flows of varying magnitudes that were stripped and overspilled from axial channels. Higher-magnitude flows repeatedly deflected and reflected against the high-relief canyon margin, suggesting that flows were completely confined within the canyon. Flows were also disrupted by dynamic relief generated by slides, debrites, and scour surfaces on the canyon floor. The canyon-confined overbank deposits then underwent a rapid stratigraphic change, likely as a result of basinward tilting inducing a more aggradational phase. In conjunction with canyon widening, this led to the overbank exhibiting a marked increase in smaller-magnitude, rapidly decelerated transitional flows that entrained mud-rich substrate. Such flows rarely interacted with the canyon margin in contrast to the lower parts of the overbank. Lateral transitions between transitional flow bed types with distance from channel elements point to unusually rapid flow transformations from turbulent to upper transitional plug flow conditions over 100–200 m, which are more rapid than observed in more basinward settings. In quiescent parts of the upper overbank, sediments reworked by internal tides are preserved, which are unique to canyon settings. This record of canyon-confined overbank deposits shares affinities with the deposits of modern canyon terraces, albeit there is a paucity of cores in modern systems and these are short. In particular, comparison with the present dataset enables identification of potential TFDs from modern canyon terraces for the first time.

Our findings suggest the existing twofold interpretation of internal levee or terrace deposits may be oversimplified in shelf-proximal submarine canyons, where such deposits may not develop as discrete subenvironments. Canyon-confined overbanks are heterolithic but exhibit particularly complex facies distributions with limited development of discrete architectural elements. This is due to deep entrenchment and associated steep confining slopes, which limit the filtering of sediment gravity flows that would normally escape the conduit in more distal settings. The nature of the overbank shifts with respect to the migration of adjacent channel elements through time and as a consequence of larger-scale external drivers such as tectonism, which further leads to a wide range of distinct flow types and deposits. This is the first bed-scale documentation of a canyon-confined overbank succession. While canyon axes are dominated by bypass and erosion, canyon-confined overbanks preserve key characteristics and a more complete record of a maturing canyon system. Therefore, our findings support the potential of these underutilized successions as cryptic, yet important, archives of submarine canyon evolution.

ACKNOWLEDGMENTS

The SLOPE 5 consortium (BP, Aker BP, CNOOC International, DNO, Harbour Energy, Hess, Murphy, Neptune Energy, Petrobras, Vår Energi, and Woodside) is thanked for its financial support. We would like to thank reviewers Zane Jobe and Andrea Fildani, Associate Editor Lawrence Tanner, and Science Editor David Fastovsky for their detailed and insightful comments that greatly improved this manuscript.

REFERENCES CITED

Abd El-Gawad, S.M., Pirmez, C., Cantelli, A., Minisini, D., Sylvester, Z., and Imran, J., 2012, 3-D numerical simulation of turbidity currents in submarine canyons off the Niger Delta: Marine Geology, v. 326–328, p. 55–66, https://doi.org/10.1016/j.margeo.2012.06.003.

Allen, J.R.L., 1971, Instantaneous sediment deposition rates deduced from climbing-ripple cross-lamination: Journal of the Geological Society, v. 127, p. 553–561, https://doi.org/10.1144/GSL.JGS.1971.127.06.02.

Allen, J.R.L., 1973, A classification of climbing-ripple cross-lamination: Journal of the Geological Society, v. 129, p. 537–541, https://doi.org/10.1144/gsjgs.129.5.0537.

Allen, J.R.L., 1984, Parallel lamination developed from upper-stage plane beds: A model based on the larger coherent structures of the turbulent boundary layer: Sedimentary Geology, v. 39, p. 227–242, https://doi.org/10.1016/0037-0738(84)90052-6.

Amaro, T., et al., 2016, The Whittard Canyon—A case study of submarine canyon processes: Progress in Oceanography, v. 146, p. 38–57, https://doi.org/10.1016/j.pocean.2016.06.003.

Amos, K.J., Peakall, J., Bradbury, P.W., Roberts, M., Keevil, G., and Gupta, S., 2010, The influence of bend amplitude and planform morphology on flow and sedimentation in submarine channels: Marine and Petroleum Geology, v. 27, p. 1431–1447, https://doi.org/10.1016/j.marpetgeo.2010.05.004.

Anderson, K.S., Graham, S.A., and Hubbard, S.M., 2006, Facies, architecture, and origin of a reservoir-scale sand-rich succession within submarine canyon fill: Insights from Wagon Caves Rock (Paleocene), Santa Lucia Range, California, U.S.A.: Journal of Sedimentary Research, v. 76, p. 819–838, https://doi.org/10.2110/jsr.2006.066.

Archer, A.W., 1996, Reliability of lunar orbital periods extracted from ancient cyclic tidal rhythmites: Earth and Planetary Science Letters, v. 141, p. 1–10, https://doi.org/10.1016/0012-821X(96)00063-5.

Arzola, R.G., Wynn, R.B., Lastras, G., Masson, D.G., and Weaver, P.P.E., 2008, Sedimentary features and processes in the Nazaré and Setúbal submarine canyons, west Iberian margin: Marine Geology, v. 250, p. 64–88, https://doi.org/10.1016/j.margeo.2007.12.006.

Ashley, G.M., Southard, J.B., and Boothroyd, J.C., 1982, Deposition of climbing-ripple beds: A flume simulation: Sedimentology, v. 29, p. 67–79, https://doi.org/10.1111/j.1365-3091.1982.tb01709.x.

Baas, J.H., and Best, J.L., 2002, Turbulence modulation in clay-rich sediment-laden flows and some implications for sediment deposition: Journal of Sedimentary Research, v. 72, p. 336–340, https://doi.org/10.1306/120601720336.

Baas, J.H., Best, J.L., Peakall, J., and Wang, M., 2009, A phase diagram for turbulent, transitional, and laminar clay suspension flows: Journal of Sedimentary Research, v. 79, p. 162–183, https://doi.org/10.2110/jsr.2009.025.

Baas, J.H., Best, J.L., and Peakall, J., 2011, Depositional processes, bedform development and hybrid bed formation in rapidly decelerated cohesive (mud-sand) sediment flows: Sedimentology, v. 58, p. 1953–1987, https://doi.org/10.1111/j.1365-3091.2011.01247.x.

Baas, J.H., Best, J.L., and Peakall, J., 2016, Predicting bedforms and primary current stratification in cohesive mixtures of mud and sand: Journal of the Geological Society, v. 173, p. 12–45, https://doi.org/10.1144/jgs2015-024.

Baas, J.H., Best, J.L., and Peakall, J., 2021a, Rapid gravity flow transformation revealed in a single climbing ripple: Geology, v. 49, p. 493–497, https://doi.org/10.1130/G48181.1.

Baas, J.H., Tracey, N.D., and Peakall, J., 2021b, Sole marks reveal deep-marine depositional process and environment: Implications for flow transformation and hybrid-event-bed models: Journal of Sedimentary Research, v. 91, p. 986–1009, https://doi.org/10.2110/jsr.2020.104.

Babonneau, N., Savoye, B., Cremer, M., and Klein, B., 2002, Morphology and architecture of the present canyon and channel system of the Zaire deep-sea fan: Marine and Petroleum Geology, v. 19, p. 445–467, https://doi.org/10.1016/S0264-8172(02)00009-0.

Babonneau, N., Savoye, B., Cremer, M., and Bez, M., 2004, Multiple terraces within the deep incised Zaire Valley (ZaïAngo Project): Are they confined levees?, *in* Lomas, S.A., and Joseph, P., eds., Confined Turbidite Systems: Geological Society, London, Special Publication 222, p. 91–114, https://doi.org/10.1144/GSL.SP.2004.222.01.06.

Babonneau, N., Savoye, B., Cremer, M., and Bez, M., 2010, Sedimentary architecture in meanders of a submarine channel: Detailed study of the present Congo turbidite channel (ZaiAngo project): Journal of Sedimentary Research, v. 80, p. 852–866, https://doi.org/10.2110/jsr.2010.078.

Bain, H.A., and Hubbard, S.M., 2016, Stratigraphic evolution of a long-lived submarine channel system in the Late Cretaceous Nanaimo Group, British Columbia, Canada: Sedimentary Geology, v. 337, p. 113–132, https://doi.org/10.1016/j.sedgeo.2016.03.010.

Baker, M.L., and Baas, J.H., 2020, Mixed sand–mud bedforms produced by transient turbulent flows in the fringe of submarine fans: Indicators of flow transformation: Sedimentology, v. 67, p. 2645–2671, https://doi.org/10.1111/sed.12714.

Baker, M.L., and Baas, J.H., 2023, Does sand promote or hinder the mobility of cohesive sediment gravity flows?: Sedimentology, v. 70, p. 1110–1130, https://doi.org/10.1111/sed.13072.

Baztan, J., Berné, S., Olivet, J.-L., Rabineau, M., Aslanian, D., Gaudin, M., Réhault, J.-P., and Canals, M., 2005, Axial incision: The key to understand submarine canyon evolution (in the western Gulf of Lion): Marine and Petroleum Geology, v. 22, p. 805–826, https://doi.org/10.1016/j.marpetgeo.2005.03.011.

Beaubouef, R.T., 2004, Deep-water leveed-channel complexes of the Cerro Toro Formation, Upper Cretaceous, southern Chile: AAPG Bulletin, v. 88, p. 1471–1500, https://doi.org/10.1306/06210403130.

Bell, D., Stevenson, C.J., Kane, I.A., Hodgson, D.M., and Poyatos-Moré, M., 2018, Topographic controls on the development of contemporaneous but contrasting basin-floor depositional architectures: Journal of Sedimentary Research, v. 88, p. 1166–1189, https://doi.org/10.2110/jsr.2018.58.

Best, J., and Bridge, J., 1992, The morphology and dynamics of low amplitude bedwaves upon upper stage plane beds and the preservation of planar laminae: Sedimentology, v. 39, p. 737–752, https://doi.org/10.1111/j.1365-3091.1992.tb02150.x.

Boehlke, J.E., and Abbott, P.L., 1986, Punta Baja Formation, a Campanian submarine canyon fill, Baja California, Mexico, *in* Abbott, P.L., ed., Cretaceous Stratigraphy, Western North America: Los Angeles, California, USA, Pacific Section, Society of Economic Paleontologists and Mineralogists, p. 91–101.

Boulesteix, K., Poyatos-Moré, M., Flint, S.S., Taylor, K.G., Hodgson, D.M., and Hasiotis, S.T., 2019, Transport and deposition of mud in deep-water environments: Processes and stratigraphic implications: Sedimentology, v. 66, p. 2894–2925, https://doi.org/10.1111/sed.12614.

Boulesteix, K., Poyatos-Moré, M., Flint, S.S., Hodgson, D.M., Taylor, K.G., and Brunt, R.L., 2022, Sedimentologic and stratigraphic criteria to distinguish between basin-floor and slope mudstones: Implications for the delivery of mud to deep-water environments: The Depositional Record, v. 8, p. 958–988, https://doi.org/10.1002/dep2.191.

Bouma, A.H., 1962, Sedimentology of Some Flysch Deposits: A Graphic Approach to Facies Interpretation: Amsterdam, Netherlands, Elsevier, 168 p.

Bouwmeester, M.J., et al., 2025, Evolution and architecture of an exhumed ocean-facing coarse-grained submarine canyon fill, Baja California, Mexico: Sedimentology, v. 72, p. 189–226, https://doi.org/10.1111/sed.13231.

Busby, C., 2004, Continental growth at convergent margins facing large ocean basins: A case study from Mesozoic convergent-margin basins of Baja California, Mexico: Tectonophysics, v. 392, p. 241–277, https://doi.org/10.1016/j.tecto.2004.04.017.

Busby, C., Smith, D., Morris, W., and Fackler-Adams, B., 1998, Evolutionary model for convergent margins facing large ocean basins: Mesozoic Baja California, Mexico: Geology, v. 26, p. 227–230, https://doi.org/10.1130/0091-7613(1998)026<0227:EMFCMF>2.3.CO;2.

Cerrillo-Escoriza, J., et al., 2024, Variable downcanyon morphology controlling the recent activity of shelf-incised submarine canyons (Alboran Sea, western Mediterranean): Geomorphology, v. 453, https://doi.org/10.1016/j.geomorph.2024.109127.

Chen, P., Kane, I.A., Clare, M.A., Soutter, E.L., Mienis, F., Wogelius, R.A., and Keavney, E., 2025, Direct evidence that microplastics are transported to the deep sea by turbidity currents: Environmental Science & Technology, v. 59, p. 7278–7287, https://doi.org/10.1021/acs.est.4c12007.

Clift, P.D., Giosan, L., Henstock, T.J., and Tabrez, A.R., 2014, Sediment storage and reworking on the shelf and in the Canyon of the Indus River-Fan System since the last glacial maximum: Basin Research, v. 26, p. 183–202, https://doi.org/10.1111/bre.12041.

Clifton, H.E., 1984, Sedimentation units in stratified resedimented conglomerate, Paleocene submarine canyon fill, Point Lobos, California, *in* Koster, E.H., and Steel, R.J., eds., Sedimentology of Gravels and Conglomerates: Canadian Society of Petroleum Geologists Memoir 10, p. 429–441.

Conway, K.W., Barrie, J.V., Picard, K., and Bornhold, B.D., 2012, Submarine channel evolution: Active channels in fjords, British Columbia, Canada: Geo-Marine Letters, v. 32, p. 301–312, https://doi.org/10.1007/s00367-012-0280-4.

Covault, J.A., Kostic, S., Paull, C.K., Sylvester, Z., and Fildani, A., 2017, Cyclic steps and related supercritical bedforms: Building blocks of deep-water depositional systems, western North America: Marine Geology, v. 393, p. 4–20, https://doi.org/10.1016/j.margeo.2016.12.009.

Cronin, B.T., and Kidd, R.B., 1998, Heterogeneity and lithotype distribution in ancient deep-sea canyons: Point Lobos deep-sea canyon as a reservoir analogue: Sedimentary Geology, v. 115, p. 315–349, https://doi.org/10.1016/S0037-0738(97)00099-7.

de Almeida, N.M., Vital, H., and Gomes, M.P., 2015, Morphology of submarine canyons along the continental margin of the Potiguar Basin, NE Brazil: Marine and Petroleum Geology, v. 68, p. 307–324, https://doi.org/10.1016/j.marpetgeo.2015.08.035.

Deptuck, M.E., Sylvester, Z., Pirmez, C., and O'Byrne, C., 2007, Migration–aggradation history and 3-D seismic geomorphology of submarine channels in the Pleistocene Benin-major Canyon, western Niger Delta slope: Marine and Petroleum Geology, v. 24, p. 406–433, https://doi.org/10.1016/j.marpetgeo.2007.01.005.

Di Celma, C., Cantalamessa, G., Didaskalou, P., and Lori, P., 2010, Sedimentology, architecture, and sequence stratigraphy of coarse-grained, submarine canyon fills from the Pleistocene (Gelasian-Calabrian) of the Peri-Adriatic basin, central Italy: Marine and Petroleum Geology, v. 27, p. 1340–1365, https://doi.org/10.1016/j.marpetgeo.2010.05.011.

Di Celma, C.N., Brunt, R.L., Hodgson, D.M., Flint, S.S., and Kavanagh, J.P., 2011, Spatial and temporal evolution of a Permian submarine slope channel–levee system, Karoo Basin, South Africa: Journal of Sedimentary Research, v. 81, p. 579–599, https://doi.org/10.2110/jsr.2011.49.

Dykstra, M., 2012, Deep-water tidal sedimentology, *in* Davis, R.A., Jr., and Dalrymple, R.W., eds., Principles of Tidal Sedimentology: Springer, Dordrecht, p. 371–395, https://doi.org/10.1007/978-94-007-0123-6_14.

Dykstra, M., and Kneller, B., 2009, Lateral accretion in a deep-marine channel complex: Implications for channelized flow processes in turbidity currents: Sedimentology, v. 56, p. 1411–1432, https://doi.org/10.1111/j.1365-3091.2008.01040.x.

Engebretson, D.C., Cox, A., and Gordon, R.G., 1985, Relative Motions Between Oceanic and Continental Plates in the Pacific Basin: Geological Society of America Special Paper 206, 59 p., https://doi.org/10.1130/SPE206.

Fildani, A., 2017, Submarine canyons: A brief review looking forward: Geology, v. 45, p. 383–384, https://doi.org/10.1130/focus042017.1.

Gardner, W.D., 1989, Periodic resuspension in Baltimore canyon by focusing of internal waves: Journal of Geophysical Research: Oceans, v. 94, p. 18,185–18,194, https://doi.org/10.1029/JC094iC12p18185.

Gastil, R.G., Philips, R.P., and Allison, E.C., 1975. Reconnaissance Geology of the State of Baja California: Geological Society of America Memoir 140, 170 p., https://doi.org/10.1130/MEM140.

Ge, Z., Nemec, W., Gawthorpe, R.L., and Hansen, E.W.M., 2017, Response of unconfined turbidity current to normal-fault topography: Sedimentology, v. 64, p. 932–959, https://doi.org/10.1111/sed.12333.

Gladstone, C., McClelland, H.L.O., Woodcock, N.H., Pritchard, D., and Hunt, J.E., 2018, The formation of convolute lamination in mud-rich turbidites: Sedimentology, v. 65, p. 1800–1825, https://doi.org/10.1111/sed.12447.

Glazner, A.F., 1991, Plutonism, oblique subduction, and continental growth: An example from the Mesozoic of California: Geology, v. 19, p. 784–786, https://doi.org/10.1130/0091-7613(1991)019<0784:POSACG>2.3.CO;2.

Guiastrennec-Faugas, L., Gillet, H., Silva Jacinto, R., Dennielou, B., Hanquiez, V., Schmidt, S., Simplet, L., and Rousset, A., 2020, Upstream migrating knickpoints and related sedimentary processes in a submarine canyon from a rare 20-year morphobathymetric time-lapse (Capbreton submarine canyon, Bay of Biscay, France): Marine Geology, v. 423, https://doi.org/10.1016/j.margeo.2020.106143.

Hall, R.A., Aslam, T., and Huvenne, V.A.I., 2017, Partly standing internal tides in a dendritic submarine canyon observed by an ocean glider: Deep-Sea Research Part I: Oceanographic Research Papers, v. 126, p. 73–84, https://doi.org/10.1016/j.dsr.2017.05.015.

Hansen, L., Callow, R., Kane, I., and Kneller, B., 2017, Differentiating submarine channel-related thin-bedded turbidite facies: Outcrop examples from the Rosario Formation, Mexico: Sedimentary Geology, v. 358, p. 19–34, https://doi.org/10.1016/j.sedgeo.2017.06.009.

Hansen, L.A.S., Callow, R.H.T., Kane, I.A., Gamberi, F., Rovere, M., Cronin, B.T., and Kneller, B.C., 2015, Genesis and character of thin-bedded turbidites associated with submarine channels: Marine and Petroleum Geology, v. 67, p. 852–879, https://doi.org/10.1016/j.marpetgeo.2015.06.007.

Harms, J.C., 1969, Hydraulic significance of some sand ripples: Geological Society of America Bulletin, v. 80, p. 363–396, https://doi.org/10.1130/0016-7606(1969)80[363:HSOSSR]2.0.CO;2.

Harris, P.T., Macmillan-Lawler, M., Rupp, J., and Baker, E.K., 2014, Geomorphology of the oceans: Marine Geology, v. 352, p. 4–24, https://doi.org/10.1016/j.margeo.2014.01.011.

Haughton, P.D.W., 1994, Deposits of deflected and ponded turbidity currents, Sorbas Basin, Southeast Spain: Journal of Sedimentary Research, v. 64, p. 233–246, https://doi.org/10.1306/D4267D6B-2B26-11D7-8648000102C1865D.

Haughton, P.D.W., Barker, S.P., and McCaffrey, W.D., 2003, 'Linked' debrites in sand-rich turbidite systems—Origin and significance: Sedimentology, v. 50, p. 459–482, https://doi.org/10.1046/j.1365-3091.2003.00560.x.

He, Y.-B., Luo, J.-X., Li, X.-D., Gao, Z.-Z., and Wen, Z., 2011, Evidence of internal-wave and internal-tide deposits in the Middle Ordovician Xujiajuan Formation of the Xiangshan Group, Ningxia, China: Geo-Marine Letters, v. 31, p. 509–523, https://doi.org/10.1007/s00367-011-0253-z.

Heezen, B.C., and Ewing, W.M., 1952, Turbidity currents and submarine slumps, and the 1929 Grand Banks [Newfoundland] earthquake: American Journal of Science, v. 250, p. 849–873, https://doi.org/10.2475/ajs.250.12.849.

Hein, F.J., and Walker, R.G., 1982, The Cambro-Ordovician Cap Enragé Formation, Québec, Canada: Conglomeratic deposits of a braided submarine channel with terraces: Sedimentology, v. 29, p. 309–352, https://doi.org/10.1111/j.1365-3091.1982.tb01798.x.

Hesse, R., Klaucke, I., Khodabakhsh, S., Piper, D.J.W., Ryan, W.B.F., and NAMOC Study Group, 2001, Sandy submarine braid plains: Potential deep-water reservoirs: AAPG Bulletin, v. 85, p. 1499–1521, https://doi.org/10.1306/8626CAEB-173B-11D7-8645000102C1865D.

Hiscott, R.N., Hall, F.R., and Pirmez, C., 1997, Turbidity-current overspill from the Amazon channel: Texture of the silt/sand load, paleoflow from anisotropy of magnetic susceptibility and implications for flow processes, *in* Flood, R.D., et al., eds., Proceedings of the Ocean Drilling Program, Scientific Results, Volume 155: College Station, Texas, USA, Ocean Drilling Program, p. 53–78.

Hofstra, M., Peakall, J., Hodgson, D.M., and Stevenson, C.J., 2018, Architecture and morphodynamics of subcritical sediment waves in an ancient channel-lobe transition zone: Sedimentology, v. 65, p. 2339–2367, https://doi.org/10.1111/sed.12468.

Hubbard, S.M., Covault, J.A., Fildani, A., and Romans, B.W., 2014, Sediment transfer and deposition in slope channels: Deciphering the record of enigmatic deep-sea processes from outcrop: Geological Society of America Bulletin, v. 126, p. 857–871, https://doi.org/10.1130/B30996.1.

Hubbard, S.M., Jobe, Z.R., Romans, B.W., Covault, J.A., Sylvester, Z., and Fildani, A., 2020, The stratigraphic evolution of a submarine channel: Linking seafloor dynamics to depositional products: Journal of Sedimentary Research, v. 90, p. 673–686, https://doi.org/10.2110/jsr.2020.36.

Ito, M., Ishikawa, K., and Nishida, N., 2014, Distinctive erosional and depositional structures formed at a canyon mouth: A lower Pleistocene deep-water succession in the Kazusa forearc basin on the Boso Peninsula, Japan: Sedimentology, v. 61, p. 2042–2062, https://doi.org/10.1111/sed.12128.

Jackson, C.A.-L., McAndrew, A.E., Hodgson, D.M., and Dreyer, T., 2021, Repeated degradation and progradation of a submarine slope over geological timescales: Journal of Sedimentary Research, v. 91, p. 116–145, https://doi.org/10.2110/jsr.2020.77.

Janocko, J., and Basilici, G., 2021, Architecture of coarse-grained gravity flow deposits in a structurally confined submarine canyon (late Eocene Tokaren Conglomerate, Slovakia): Sedimentary Geology, v. 417, https://doi.org/10.1016/j.sedgeo.2021.105880.

Jobe, Z., Sylvester, Z., Bolla Pittaluga, M., Frascati, A., Pirmez, C., Minisini, D., Howes, N., and Cantelli, A., 2017, Facies architecture of submarine channel deposits on the western Niger Delta slope: Implications for grain-size and density stratification in turbidity currents: Journal of Geophysical Research: Earth Surface, v. 122, p. 473–491, https://doi.org/10.1002/2016JF003903.

Jobe, Z.R., Lowe, D.R., and Morris, W.R., 2012, Climbing-ripple successions in turbidite systems: Depositional environments, sedimentation rates and accumulation times: Sedimentology, v. 59, p. 867–898, https://doi.org/10.1111/j.1365-3091.2011.01283.x.

Jobe, Z.R., Sylvester, Z., Parker, A.O., Howes, N., Slowey, N., and Pirmez, C., 2015, Rapid adjustment of submarine channel architecture to changes in sediment supply: Journal of Sedimentary Research, v. 85, p. 729–753, https://doi.org/10.2110/jsr.2015.30.

Jobe, Z.R., Hubbard, S.M., and Romans, B.W., 2024, How many turbidity currents pass through a submarine channel during its lifespan?: Journal of Sedimentary Research, v. 94, p. 737–749, https://doi.org/10.2110/jsr.2024.050.

Jopling, A.V., and Walker, R.G., 1968, Morphology and origin of ripple-drift cross-lamination, with examples from the Pleistocene of Massachusetts: Journal of Sedimentary Research, v. 38, p. 971–984, https://doi.org/10.1306/74D71ADC-2B21-11D7-8648000102C1865D.

Kane, I.A., and Hodgson, D.M., 2011, Sedimentological criteria to differentiate submarine channel levee subenvironments: Exhumed examples from the Rosario Fm. (Upper Cretaceous) of Baja California, Mexico, and the Fort Brown Fm. (Permian), Karoo Basin, S. Africa: Marine and Petroleum Geology, v. 28, p. 807–823, https://doi.org/10.1016/j.marpetgeo.2010.05.009.

Kane, I.A., Dykstra, M.L., Kneller, B.C., Tremblay, S., and McCaffrey, W.D., 2009, Architecture of a coarse-grained channel–levée system: The Rosario Formation, Baja California, Mexico: Sedimentology, v. 56, p. 2207–2234, https://doi.org/10.1111/j.1365-3091.2009.01077.x.

Kane, I.A., Hodgson, D.M., Hubbard, S.M., McArthur, A.D., Poyatos-Moré, M., Soutter, E.L., Flint, S.S., and Matthews, W., 2022, Deep-water tectono-stratigraphy at a plate boundary constrained by large n-detrital zircon and micropaleontological approaches: Peninsular Ranges forearc, Baja California, Mexico: The Sedimentary Record, v. 20, no. 1, https://doi.org/10.2110/001c.37652.

Keavney, E., Peakall, J., Wang, R., Hodgson, D.M., Kane, I.A., Keevil, G.M., Brown, H.C., Clare, M.A., and Hughes, M.J., 2025a, Unconfined gravity current interactions with orthogonal topography: Implications for combined-flow processes and the depositional record: Sedimentology, v. 72, p. 67–99, https://doi.org/10.1111/sed.13227.

Keavney, E., Kane, I.A., Clare, M.A., Hodgson, D.M., Huvenne, V.A.I., Sumner, E.J., Peakall, J., Mienis, F., and Kranenburg, J., 2025b, The combined role of near-bed currents and sub-seafloor processes in the transport and pervasive burial of microplastics in submarine canyons: Journal of the Geological Society, v. 182, https://doi.org/10.1144/jgs2024-228.

Keevil, G.M., Peakall, J., Best, J.L., and Amos, K.J., 2006, Flow structure in sinuous submarine channels: Velocity and turbulence structure of an experimental submarine channel: Marine Geology, v. 229, p. 241–257, https://doi.org/10.1016/j.margeo.2006.03.010.

Kilmer, F.H., 1963, Cretaceous and Cenozoic stratigraphy and paleontology, El Rosario area, Baja California, Mexico [Ph.D. thesis]: Berkeley, California, USA, University of California, 216 p.

Kimbrough, D.L., Smith, D.P., Mahoney, J.B., Moore, T.E., Grove, M., Gastil, R.G., Ortega-Rivera, A., and Fanning, C.M., 2001, Forearc-basin sedimentary response to rapid Late Cretaceous batholith emplacement in the Peninsular Ranges of southern and Baja California: Geology, v. 29, p. 491–494, https://doi.org/10.1130/0091-7613(2001)029<0491:FBSRTR>2.0.CO;2.

Klaucke, I., and Hesse, R., 1996, Fluvial features in the deep-sea: New insights from the glacigenic submarine drainage system of the Northwest Atlantic Mid-Ocean Channel in the Labrador Sea: Sedimentary Geology, v. 106, p. 223–234, https://doi.org/10.1016/S0037-0738(96)00008-5.

Kneller, B., 1995, Beyond the turbidite paradigm: Physical models for deposition of turbidites and their implications for reservoir prediction, *in* Hartley, A.J., and Prosser, D.J., eds., Characterization of Deep Marine Clastic Systems: Geological Society, London, Special Publication 94, p. 31–49, https://doi.org/10.1144/GSL.SP.1995.094.01.04.

Kneller, B., 2003, The influence of flow parameters on turbidite slope channel architecture: Marine and Petroleum Geology, v. 20, p. 901–910, https://doi.org/10.1016/j.marpetgeo.2003.03.001.

Kneller, B., and Buckee, C., 2000, The structure and fluid mechanics of turbidity currents: A review of some recent studies and their geological implications: Sedimentology, v. 47, no. s1, p. 62–94, https://doi.org/10.1046/j.1365-3091.2000.047s1062.x.

Kneller, B., Bozetti, G., Callow, R., Dykstra, M., Hansen, L., Kane, I., Li, P., McArthur, A., Santa Catharina, A., Dos Santos, T., and Thompson, P., 2020, Architecture, process, and environmental diversity in a late Cretaceous slope channel system: Journal of Sedimentary Research, v. 90, p. 1–26, https://doi.org/10.2110/jsr.2020.1.

Kneller, B.C., and Branney, M.J., 1995, Sustained high-density turbidity currents and the deposition of thick massive sands: Sedimentology, v. 42, p. 607–616, https://doi.org/10.1111/j.1365-3091.1995.tb00395.x.

Kuenen, P.H., 1966, Experimental turbidite lamination in a circular flume: The Journal of Geology, v. 74, p. 523–545, https://doi.org/10.1086/627187.

Li, M.Z., Prescott, R.H., and Robertson, A.G., 2019, Observation of internal tides and sediment transport processes at the head of Logan Canyon on central Scotian Slope, eastern Canada: Journal of Marine Systems, v. 193, p. 103–125, https://doi.org/10.1016/j.jmarsys.2019.02.007.

Li, S., Li, W., Alves, T.M., Wang, J., Feng, Y., Sun, J., Li, J., and Wu, S., 2020, Large-scale scours formed by supercritical turbidity currents along the full length of a submarine canyon, northeast South China Sea: Marine Geology, v. 424, https://doi.org/10.1016/j.margeo.2020.106158.

Li, Y., and Clift, P.D., 2023, Controls on grain-size variability in the Holocene fill of the Indus Submarine Canyon: Journal of Sedimentary Research, v. 93, p. 71–87, https://doi.org/10.2110/jsr.2022.038.

Lowe, D., 1972, Submarine canyon and slope channel sedimentation model as inferred from Upper Cretaceous deposits, western California, *in* Proceedings, 24th International Geological Congress, Montreal, Québec, Canada, v. 6, p. 75–81.

Lowe, D.R., 1982, Sediment gravity flows: II. Depositional models with special reference to the deposits of high-density turbidity currents: Journal of Sedimentary Petrology, v. 52, p. 279–297, https://doi.org/10.1306/212F7F31-2B24-11D7-8648000102C1865D.

Lowe, D.R., and Guy, M., 2000, Slurry-flow deposits in the Britannia Formation (Lower Cretaceous), North Sea: A new perspective on the turbidity current and debris flow problem: Sedimentology, v. 47, p. 31–70, https://doi.org/10.1046/j.1365-3091.2000.00276.x.

Lowe, D.R., Graham, S.A., Malkowski, M.A., and Das, B., 2019, The role of avulsion and splay development in deep-water channel systems: Sedimentology, architecture, and evolution of the deep-water Pliocene Godavari "A" channel complex, India: Marine and Petroleum Geology, v. 105, p. 81–99, https://doi.org/10.1016/j.marpetgeo.2019.04.010.

Maier, K.L., Fildani, A., McHargue, T.R., Paull, C.K., Graham, S.A., and Caress, D.W., 2012, Punctuated deep-water channel migration: High-resolution subsurface data from the Lucia Chica channel system, offshore California, U.S.A.: Journal of Sedimentary Research, v. 82, p. 1–8, https://doi.org/10.2110/jsr.2012.10.

Maier, K.L., Johnson, S.Y., and Hart, P., 2018, Controls on submarine canyon head evolution: Monterey Canyon, offshore central California: Marine Geology, v. 404, p. 24–40, https://doi.org/10.1016/j.margeo.2018.06.014.

Maier, K.L., et al., 2019, Sediment and organic carbon transport and deposition driven by internal tides along Monterey Canyon, offshore California: Deep-Sea Research Part I: Oceanographic Research Papers, v. 153, https://doi.org/10.1016/j.dsr.2019.103108.

May, J.A., and Warme, J.E., 2000, Bounding surfaces, lithologic variability, and sandstone connectivity within submarine-canyon outcrops, Eocene of San Diego, California, *in* Weimer, P., ed., Deep-Water Reservoirs of the World: Gulf Coast Section, Society for Sedimentary Geology (SEPM), p. 556–577, https://doi.org/10.5724/gcs.00.15.0556.

McArthur, A., Kane, I., Bozetti, G., Hansen, L., and Kneller, B.C., 2020, Supercritical flows overspilling from bypass-dominated submarine channels and the development of overbank bedforms: The Depositional Record, v. 6, p. 21–40, https://doi.org/10.1002/dep2.78.

McArthur, A.D., and McCaffrey, W.D., 2019, Sedimentary architecture of detached deep-marine canyons: Examples from the East Coast Basin of New Zealand: Sedimentology, v. 66, p. 1067–1101, https://doi.org/10.1111/sed.12536.

McGee, D.C., 1965, Upper Cretaceous (Campanian) Foraminiferida from Punta Baja, Baja California [abs.]: AAPG Bulletin, v. 49, no. 7, p. 1087, https://doi.org/10.1306/A66336DC-16C0-11D7-8645000102C1865D.

McHargue, T., Pyrcz, M.J., Sullivan, M.D., Clark, J.D., Fildani, A., Romans, B.W., Covault, J.A., Levy, M., Posamentier, H.W., and Drinkwater, N.J., 2011, Architecture of turbidite channel systems on the continental slope: Patterns and predictions: Marine and Petroleum Geology, v. 28, p. 728–743, https://doi.org/10.1016/j.marpetgeo.2010.07.008.

Mercier, L., Migeon, S., Rubino, J.-L., Rojas-Agramonte, Y., Hagen, A., Bousquet, R., and Mertz-Kraus, R., 2026, A mud-filled submarine canyon cutting through a sand-prone turbidite succession: A Lower Oligocene field analogue of stratigraphic-structural trap in the Western Alpine Foreland Basin, France: Marine and Petroleum Geology, v. 183, https://doi.org/10.1016/j.marpetgeo.2025.107620.

Millington, J.J., and Clark, J.D., 1995, The Charo/Arro canyon-mouth sheet system, south-central Pyrenees, Spain: A structurally influenced zone of sediment dispersal: Journal of Sedimentary Research, v. 65, p. 443–454, https://doi.org/10.1306/D426827F-2B26-11D7-8648000102C1865D.

Morris, E.A., Hodgson, D.M., Flint, S., Brunt, R.L., Luthi, S.M., and Kolenberg, Y., 2016, Integrating outcrop and subsurface data to assess the temporal evolution of a submarine channel–levee system: AAPG Bulletin, v. 100, p. 1663–1691, https://doi.org/10.1306/04271615056.

Morris, W.R., and Busby, C.J., 1996, The effects of tectonism on the high resolution sequence stratigraphic framework of non-marine to deep-marine deposits in the Peninsular Ranges forearc basin complex, *in* Abbott, P.L., and Cooper, J.D., eds., Field Conference Guidebook and Volume for the American Association of Petroleum Geologists Annual Convention, San Diego, California, May 1996: Pacific Section, American Association of Petroleum Geologists Guidebook 73, p. 381–408, https://doi.org/10.32375/1996-GB73.19.

Morris, W.R., and Busby-Spera, C.J., 1988, Sedimentologic evolution of a submarine canyon in a forearc basin, Upper Cretaceous Rosario Formation, San Carlos, Mexico: AAPG Bulletin, v. 72, p. 717–737, https://doi.org/10.1306/703C8F0B-1707-11D7-8645000102C1865D.

Morris, W.R., and Busby-Spera, C., 1990, A submarine-fan valley-levee complex in the Upper Cretaceous Rosario Formation: Implication for turbidite facies models: Geological Society of America Bulletin, v. 102, p. 900–914, https://doi.org/10.1130/0016-7606(1990)102<0900:ASFVLC>2.3.CO;2.

Mountjoy, J.J., et al., 2018, Earthquakes drive large-scale submarine canyon development and sediment supply to deep-ocean basins: Science Advances, v. 4, https://doi.org/10.1126/sciadv.aar3748.

Mutti, E., 1992, Turbidite Sandstones: Milan, San Donato, 275 p.

Mutti, E., and Normark, W.R., 1987, Comparing examples of modern and ancient turbidite systems: Problems and concepts, *in* Leggett, J.K., and Zuffa, G.G., eds., Marine Clastic Sedimentology:

Concepts and Case Studies: Springer, Dordrecht, p. 1–38, https://doi.org/10.1007/978-94-009-3241-8_1.
Normandeau, A., Dafoe, L.T., Li, M.Z., Campbell, D.C., and Jenner, K.A., 2024, Sedimentary record of bottom currents and internal tides in a modern highstand submarine canyon head: Sedimentology, v. 71, p. 1061–1083, https://doi.org/10.1111/sed.13165.
Normandeau, A., Jenner, K.A., Desiage, P.-A., De Moura Neves, B., Edinger, E., Van Nieuwenhove, N., Limoges, A., Cote, D., and Sherwood, O.A., 2025, Holocene earthquake-triggered submarine landslides and turbidites in western Baffin Bay: Canadian Journal of Earth Sciences, v. 62, p. 1043–1061, https://doi.org/10.1139/cjes-2024-0068.
Normark, W.R., Posamentier, H., and Mutti, E., 1993, Turbidite systems: State of the art and future directions: Reviews of Geophysics, v. 31, p. 91–116, https://doi.org/10.1029/93RG02832.
Patacci, M., Haughton, P.D.W., and McCaffrey, W.D., 2015, Flow behavior of ponded turbidity currents: Journal of Sedimentary Research, v. 85, p. 885–902, https://doi.org/10.2110/jsr.2015.59.
Paull, C.K., Mitts, P., Ussler, W., III, Keaten, R., and Greene, H.G., 2005, Trail of sand in upper Monterey Canyon: Offshore California: Geological Society of America Bulletin, v. 117, p. 1134–1145, https://doi.org/10.1130/B25390.1.
Paull, C.K., Caress, D.W., Lundsten, E., Gwiazda, R., Anderson, K., McGann, M., Conrad, J., Edwards, B., and Sumner, E.J., 2013, Anatomy of the La Jolla Submarine Canyon system: Offshore southern California: Marine Geology, v. 335, p. 16–34, https://doi.org/10.1016/j.margeo.2012.10.003.
Paull, C.K., et al., 2018, Powerful turbidity currents driven by dense basal layers: Nature Communications, v. 9, 4114, https://doi.org/10.1038/s41467-018-06254-6.
Peakall, J., McCaffrey, B., and Kneller, B., 2000, A process model for the evolution, morphology, and architecture of sinuous submarine channels: Journal of Sedimentary Research, v. 70, p. 434–448, https://doi.org/10.1306/2DC4091C-0E47-11D7-8643000102C1865D.
Peakall, J., Best, J., Baas, J.H., Hodgson, D.M., Clare, M.A., Talling, P.J., Dorrell, R.M., and Lee, D.R., 2020, An integrated process-based model of flutes and tool marks in deep-water environments: Implications for palaeohydraulics, the Bouma sequence and hybrid event beds: Sedimentology, v. 67, p. 1601–1666, https://doi.org/10.1111/sed.12727.
Petruncio, E.T., Rosenfeld, L.K., and Paduan, J.D., 1998, Observations of the internal tide in Monterey Canyon: Journal of Physical Oceanography, v. 28, p. 1873–1903, https://doi.org/10.1175/1520-0485(1998)028<1873:OOTITI>2.0.CO;2.
Pickering, K.T., and Corregidor, J., 2005, Mass-transport complexes (MTCs) and tectonic control on basin-floor submarine fans, middle Eocene, south Spanish Pyrenees: Journal of Sedimentary Research, v. 75, p. 761–783, https://doi.org/10.2110/jsr.2005.062.
Pickering, K.T., and Hiscott, R.N., 1985, Contained (reflected) turbidity currents from the Middle Ordovician Cloridorme Formation, Quebec, Canada: An alternative to the antidune hypothesis: Sedimentology, v. 32, p. 373–394, https://doi.org/10.1111/j.1365-3091.1985.tb00518.x.
Piper, D.J.W., and Normark, W.R., 1983, Turbidite depositional patterns and flow characteristics, Navy Submarine Fan, California Borderland: Sedimentology, v. 30, p. 681–694, https://doi.org/10.1111/j.1365-3091.1983.tb00702.x.
Pirmez, C., and Imran, J., 2003, Reconstruction of turbidity currents in Amazon Channel: Marine and Petroleum Geology, v. 20, p. 823–849, https://doi.org/10.1016/j.marpetgeo.2003.03.005.
Pope, E.L., et al., 2022, Carbon and sediment fluxes inhibited in the submarine Congo Canyon by landslide-damming: Nature Geoscience, v. 15, p. 845–853, https://doi.org/10.1038/s41561-022-01017-x.
Privat, A.M.-L.J., Peakall, J., Hodgson, D.M., Schwarz, E., Jackson, C.A.-L., and Arnol, J.A., 2024, Evolving fill-and-spill patterns across linked early post-rift depocentres control lobe characteristics: Los Molles Formation, Argentina: Sedimentology, v. 71, p. 1639–1685, https://doi.org/10.1111/sed.13190.
Renne, P.R., Fulford, M.M., and Busby-Spera, C., 1991, High resolution $^{40}Ar/^{39}Ar$ chronostratigraphy of the Late Cretaceous El Gallo Formation, Baja California del Norte, Mexico: Geophysical Research Letters, v. 18, p. 459–462, https://doi.org/10.1029/91GL00464.
Ruffell, S.C., et al., 2024, Time-lapse surveys reveal patterns and processes of erosion by exceptionally powerful turbidity currents that flush submarine canyons: A case study of the Congo Canyon: Geomorphology, v. 463, https://doi.org/10.1016/j.geomorph.2024.109350.
Satur, N., Kelling, G., Cronin, B.T., Hurst, A., and Gürbüz, K., 2005, Sedimentary architecture of a canyon-style fairway feeding a deep-water clastic system, the Miocene Cingöz Formation, southern Turkey: Significance for reservoir characterisation and modelling: Sedimentary Geology, v. 173, p. 91–119, https://doi.org/10.1016/j.sedgeo.2003.11.024.
Schwarz, E., and Arnott, R.W.C., 2007, Anatomy and evolution of a slope channel-complex set (Neoproterozoic Isaac Formation, Windermere Supergroup, southern Canadian Cordillera): Implications for reservoir characterization: Journal of Sedimentary Research, v. 77, p. 89–109, https://doi.org/10.2110/jsr.2007.015.
Shanmugam, G., 2003, Deep-marine tidal bottom currents and their reworked sands in modern and ancient submarine canyons: Marine and Petroleum Geology, v. 20, p. 471–491, https://doi.org/10.1016/S0264-8172(03)00063-1.
Shanmugam, G., and Wang, Y., 2014, Review of research in internal-wave and internal-tide deposits of China: Discussion: Journal of Palaeogeography, v. 3, p. 332–350.
Shepard, F.P., 1976, Tidal components of currents in submarine canyons: The Journal of Geology, v. 84, p. 343–350, https://doi.org/10.1086/628199.
Shepard, F.P., and Marshall, N.F., 1969, Currents in La Jolla and Scripps Submarine Canyons: Science, v. 165, p. 177–178, https://doi.org/10.1126/science.165.3889.177.
Smith, D.P., Ruiz, G., Kvitek, R., and Iampietro, P.J., 2005, Semiannual patterns of erosion and deposition in upper Monterey Canyon from serial multibeam bathymetry: Geological Society of America Bulletin, v. 117, p. 1123–1133, https://doi.org/10.1130/B25510.1.
Sohn, Y.K., 1997, On traction-carpet sedimentation: Journal of Sedimentary Research, v. 67, p. 502–509, https://doi.org/10.1306/D42685AE-2B26-11D7-8648000102C1865D.
Soutter, E.L., Bell, D., Cumberpatch, Z.A., Ferguson, R.A., Spychala, Y.T., Kane, I.A., and Eggenhuisen, J.T., 2021, The influence of confining topography orientation on experimental turbidity currents and geological implications: Frontiers of Earth Science, v. 8, https://doi.org/10.3389/feart.2020.540633.
Sprague, A.R.G., et al., 2002, The physical stratigraphy of deep-water strata: A hierarchical approach to the analysis of genetically related stratigraphic elements for improved reservoir prediction: Abstract A167 presented at American Association of Petroleum Geologists Annual Meeting, Houston, Texas, 10–13 March.
Sprague, A.R.G., et al., 2005, Integrated slope channel depositional models: The key to successful prediction of reservoir presence and quality in offshore West Africa: Paper presented at Colegio de Ingenieros Petroleros de México (CIPM) E-Exitep 2005, Veracruz, Mexico, 20–23 February.
Stanley, D.J., 1975, Submarine canyon and slope sedimentation (Grès d'Annot) in the French Maritime Alps: Paper presented at 9th International Congress of Sedimentology, Nice, France, 129 p.
Stevenson, C.J., Talling, P.J., Wynn, R.B., Masson, D.G., Hunt, J.E., Frenz, M., Akhmetzhanhov, A., and Cronin, B.T., 2013, The flows that left no trace: Very large-volume turbidity currents that bypassed sediment through submarine channels without eroding the sea floor: Marine and Petroleum Geology, v. 41, p. 186–205, https://doi.org/10.1016/j.marpetgeo.2012.02.008.
Stevenson, C.J., Jackson, C.A.-L., Hodgson, D.M., Hubbard, S.M., and Eggenhuisen, J.T., 2015, Deep-water sediment bypass: Journal of Sedimentary Research, v. 85, p. 1058–1081, https://doi.org/10.2110/jsr.2015.63.
Stevenson, C.J., Peakall, J., Hodgson, D.M., Bell, D., and Privat, A., 2020, T_B or not T_B: banding in turbidite sandstones: Journal of Sedimentary Research, v. 90, p. 821–842, https://doi.org/10.2110/jsr.2020.43.
Stow, D., and Johansson, M., 2000, Deep-water massive sands: Nature, origin and hydrocarbon implications: Marine and Petroleum Geology, v. 17, p. 145–174, https://doi.org/10.1016/S0264-8172(99)00051-3.
Sumner, E.J., Amy, L.A., and Talling, P.J., 2008, Deposit structure and processes of sand deposition from decelerating sediment suspensions: Journal of Sedimentary Research, v. 78, p. 529–547, https://doi.org/10.2110/jsr.2008.062.
Sumner, E.J., Talling, P.J., and Amy, L.A., 2009, Deposits of flows transitional between turbidity current and debris flow: Geology, v. 37, p. 991–994, https://doi.org/10.1130/G30059A.1.
Symons, W.O., Sumner, E.J., Talling, P.J., Cartigny, M.J.B., and Clare, M.A., 2016, Large-scale sediment waves and scours on the modern seafloor and their implications for the prevalence of supercritical flows: Marine Geology, v. 371, p. 130–148, https://doi.org/10.1016/j.margeo.2015.11.009.
Talling, P.J., Amy, L.A., Wynn, R.B., Peakall, J., and Robinson, M., 2004, Beds comprising debrite sandwiched within co-genetic turbidite: Origin and widespread occurrence in distal depositional environments: Sedimentology, v. 51, p. 163–194, https://doi.org/10.1111/j.1365-3091.2004.00617.x.
Talling, P.J., Masson, D.G., Sumner, E.J., and Malgesini, G., 2012, Subaqueous sediment density flows: Depositional processes and deposit types: Sedimentology, v. 59, p. 1937–2003, https://doi.org/10.1111/j.1365-3091.2012.01353.x.
Talling, P.J., et al., 2022, Longest sediment flows yet measured show how major rivers connect efficiently to deep sea: Nature Communications, v. 13, 4193, https://doi.org/10.1038/s41467-022-31689-3.

Talling, P.J., et al., 2023, Detailed monitoring reveals the nature of submarine turbidity currents: Nature Reviews Earth & Environment, v. 4, p. 642–658, https://doi.org/10.1038/s43017-023-00458-1.

Taylor, W.J., Hodgson, D.M., Peakall, J., Kane, I.A., Morris, E.A., and Flint, S.S., 2024, Unidirectional and combined transitional flow bedforms: Controls on process and distribution in submarine slope settings: Sedimentology, v. 71, p. 1329–1362, https://doi.org/10.1111/sed.13177.

Tek, D.E., McArthur, A.D., Poyatos-Moré, M., Colombera, L., Patacci, M., Craven, B., and McCaffrey, W.D., 2021, Relating seafloor geomorphology to subsurface architecture: How mass-transport deposits and knickpoint-zones build the stratigraphy of the deep-water Hikurangi Channel: Sedimentology, v. 68, p. 3141–3190, https://doi.org/10.1111/sed.12890.

Tek, D.E., McArthur, A.D., Poyatos-Moré, M., Colombera, L., Allen, C., Patacci, M., and McCaffrey, W.D., 2022, Controls on the architectural evolution of deep-water channel overbank sediment wave fields: Insights from the Hikurangi Channel, offshore New Zealand: New Zealand Journal of Geology and Geophysics, v. 65, p. 141–178, https://doi.org/10.1080/00288306.2021.1978509.

Tinterri, R., 2011, Combined flow sedimentary structures and the genetic link between sigmoidal- and hummocky-cross stratification: Geoacta, v. 10, p. 43–85.

Tinterri, R., 2025, A new turbidite facies-tract scheme including supercritical and transitional sand–mud flows: An outcrop perspective from Mediterranean-type foreland basins: Journal of Sedimentary Research, v. 95, p. 239–272, https://doi.org/10.2110/jsr.2024.033.

Tinterri, R., Mazza, T., and Magalhaes, P.M., 2022, Contained-reflected megaturbidites of the Marnoso-arenacea Formation (Contessa key bed) and helminthoid flysches (northern Apennines, Italy) and Hecho Group (south-western Pyrenees): Frontiers in Earth Sciences, v. 10, https://doi.org/10.3389/feart.2022.817012.

van Haren, H., Mienis, F., and Duineveld, G., 2022, Contrasting internal tide turbulence in a tributary of the Whittard Canyon: Continental Shelf Research, v. 236, https://doi.org/10.1016/j.csr.2022.104679.

Visser, M.J., 1980, Neap-spring cycles reflected in Holocene subtidal large-scale bedform deposits: A preliminary note: Geology, v. 8, p. 543–546, https://doi.org/10.1130/0091-7613(1980)8<543:NCRIHS>2.0.CO;2.

von Rad, U., and Tahir, M., 1997, Late Quaternary sedimentation on the outer Indus shelf and slope (Pakistan): Evidence from high-resolution seismic data and coring: Marine Geology, v. 138, p. 193–236, https://doi.org/10.1016/S0025-3227(96)00090-4.

Vrolijk, P.J., and Southard, J.B., 1997, Experiments on rapid deposition of sand from high-velocity flows: Geoscience Canada, v. 24, p. 45–54.

Wang, R., Peakall, J., Hodgson, D.M., Keavney, E., Brown, H.C. and Keevil, G.M., 2025, Three-dimensional gravity current interactions with oblique slopes: Deflection, reflection and combined-flow behaviours: Sedimentology, v. 72, p. 2121–2159, https://doi.org/10.1111/sed.70032.

Wang, Z., and Plate, E.C.H.J., 1996, A preliminary study on the turbulence structure of flows of non-Newtonian fluid: Journal of Hydraulic Research, v. 34, p. 345–361, https://doi.org/10.1080/00221689609498484.

Winterwerp, J.C., and van Kesteren, W.G.M., 2004, Flocculation processes, *in* Introduction to the Physics of Cohesive Sediment in the Marine Environment: Amsterdam, Elsevier, Developments in Sedimentology, v. 56, p. 87–119, https://doi.org/10.1016/S0070-4571(04)80005-0.

Wynn, R.B., Cronin, B.T., and Peakall, J., 2007, Sinuous deep-water channels: Genesis, geometry and architecture: Marine and Petroleum Geology, v. 24, p. 341–387, https://doi.org/10.1016/j.marpetgeo.2007.06.001.

Yang, Y., Maselli, V., Normandeau, A., Piper, D.J.W., Li, M.Z., Campbell, D.C., Gregory, T., and Gao, S., 2020, Latitudinal response of storm activity to abrupt climate change during the last 6,500 years: Geophysical Research Letters, v. 47, https://doi.org/10.1029/2020GL089859.

Zhenzhong, G., and Eriksson, K.A., 1991, Internal-tide deposits in an Ordovician submarine channel: Previously unrecognized facies?: Geology, v. 19, p. 734–737, https://doi.org/10.1130/0091-7613(1991)019<0734:ITDIAO>2.3.CO;2.

Zhong, G., and Peng, X., 2021, Transport and accumulation of plastic litter in submarine canyons—The role of gravity flows: Geology, v. 49, p. 581–586, https://doi.org/10.1130/G48536.1.